miRNA-based buffering of the cobblestone–lissencephaly-associated extracellular matrix receptor dystroglycan via its alternative *3′-UTR*

Andriy S. Yatsenko[1,*], April K. Marrone[1,*] & Halyna R. Shcherbata[1]

Many proteins are expressed dynamically during different stages of cellular life and the accuracy of protein amounts is critical for cell endurance. Therefore, cells should have a perceptive system that notifies about fluctuations in the amounts of certain components and an executive system that efficiently restores their precise levels. At least one mechanism that evolution has employed for this task is regulation of *3′-UTR* length for microRNA targeting. Here we show that in *Drosophila* the microRNA complex *miR-310s* acts as an executive mechanism to buffer levels of the muscular dystrophy-associated extracellular matrix receptor dystroglycan via its alternative *3′-UTR*. *miR-310s* gene expression fluctuates depending on dystroglycan amounts and nitric oxide signalling, which perceives dystroglycan levels and regulates microRNA gene expression. Aberrant levels of dystroglycan or deficiencies in *miR-310s* and nitric oxide signalling result in cobblestone brain appearance, resembling human lissencephaly type II phenotype.

[1] Max Planck Research Group of Gene Expression and Signaling, Max Planck Institute for Biophysical Chemistry, Am Fassberg 11, 37077 Göttingen, Germany. * These authors contributed equally to this work. Correspondence and requests for materials should be addressed to H.R.S. (email: halyna.shcherbata@mpibpc.mpg.de).

1

Developmental biologists typically are interested in phenotypes caused by gene loss-of-function; however, multiple stresses, unfavourable conditions, or developmental events can affect the precision of gene expression at the transcriptional level, resulting in altered protein levels. Elevated amounts of a critical protein can potentially be as deadly as its deficiency. In addition, the levels of numerous proteins constantly fluctuate due to different phases of cellular life, such as the cell cycle stage, cell shape rearrangements and motility. Many of the essential cellular functions are dependent on cell–extracellular matrix (ECM) contacts and are associated with cell shape reorganization[1,2]. The ECM provides signalling cues that coordinate multiple cell behaviour aspects to guarantee proper tissue formation and homeostasis[3]. The extracellular signals from the ECM to the cytoplasm are transmitted via ECM receptors (that is, integrins and dystroglycan) to activate specific signalling pathways inside the cell, modifying the gene expression programme. Conversely, changes inside the cell are transduced via these transmembrane proteins to adjust the surrounding ECM composition that in turn changes cell biochemistry[2,4]. The ECM constituents also establish a three-dimensional microenvironment that controls cell division and growth, survival and differentiation. As these processes are very dynamic, it suggests a need for a mechanism that restores proper levels of cell adhesion proteins. This mechanism should account for at least two major tasks: to sense abnormal levels of the protein and to send this information to induce a cellular response that will re-establish equilibrium.

Dystroglycan (Dg) is a conserved critical ECM receptor that is responsible for processes relevant to total organism health. It is a key component of the dystrophin (Dys) glycoprotein complex (DGC), connecting the ECM to the actin cytoskeleton via the cytoplasmic protein Dys[5–7]. The DGC is best known for its association with a large group of inherited neuromuscular diseases, muscular dystrophies. Owing to the high occurrence of these sometimes fatal diseases, the majority of research has focused on the role of the DGC in providing mechanical stability to the muscle sarcolemma to resist the vigour of contraction[6,8,9]. However, the DGC not only offers strength to the muscle sarcolemma, but also it has crucial roles in central nervous system development, as many muscular dystrophy patients experience cognitive impairment and learning disability, and develop some behavioural and neuropsychiatric disorders[10]. In particular, abnormal interaction of Dg and the ECM results in the cobblestone brain, which is an odd malformation, resulting from neuron overmigration and formation of an extracortical layer that resembles a bumpy cobblestone surface[10,11]. There are several vertebrate dystroglycanopathy models[12]; however, a Drosophila model has not been developed.

Previously, we have reported that Drosophila can serve as a great system to study muscular dystrophies and Dg deficiencies lead to muscle and nervous system disorders[13,14]. Drosophila Dg has distinct functions from Dys, and apart from its role in muscle maintenance it is involved in energy homeostasis, photoreceptor differentiation and neuromuscular junction establishment[14–18]. In addition, Dg deficiency has been shown to alter the microRNA (miRNA) profile, providing a link between the DGC and regulation of messenger RNA and protein levels[19]. Dg can be detected in various tissues in mammals and in Drosophila[13,20,21]. In both vertebrates and invertebrates, there are numerous Dg gene transcripts listed in GenBank, but it is not known why there is so much variation in the protein isoforms and what are regulatory events, including post-transcriptional control, which give rise to the mature, sugar-decorated protein. The broad expression pattern and the multiple cellular processes that Dg is being discovered to play a role in indicate that it can be

considered as an ECM housekeeping gene (reviewed in ref. 3). Therefore, it is logical that there are various forms of regulation available to manage its levels, especially in the brain, where the exactitude of ECM–cell adhesion is particularly important for brain compartmentalization and greatly contributes to the brain complexity.

Now we report that precise levels of Dg per se are critical, as lower levels slow down neuronal stem cell division, while higher levels accelerate proliferation and perturb neuron differentiation. Interestingly, altered Dg levels lead to formation of cobblestone-like structures that outgrow the normal contour of the ECM-defined brain space. This phenotype is similar to the brain cortex abnormalities associated with dystroglycanopathies in humans, implying that Drosophila Dg mutants can serve as a model for cobblestone lissencephaly. We have found that misregulation of Dg affects the distribution of major cell adhesion proteins, which presumably alters cell–ECM interaction, consequently resulting in abnormal tissue assembly. The intensity of the cobblestone-like phenotype is proportional to the amount and the duration of Dg protein misregulation. Dg is subjected to alternative 3'-UTR processing, and our evidence suggests that this is a mechanism allowing for its partial visibility to the miR-310s complex of miRNAs. This regulation is critical in response to cell shape rearrangements that take place during neuronal stem cell division, neuron differentiation, and brain morphogenesis. As a consequence of the miR-310s regulation, only a portion of Dg mRNAs with an extended 3'-UTR can be targeted, preventing Dg levels from being reduced below a certain threshold that would affect nervous system development. In addition, miR-310s levels are sensitive to those of Dg and nitric oxide (NO) signalling alike, indicating a Dg-NO-miR-310s regulatory loop. As NO signalling regulates miRNA gene expression and the cellular localization of NO signalling components per se depends on Dg, it implies that Dg is involved indirectly in transcriptional activation of its own repressors, the miR-310s. Thus, this study is an example of the proposed perceptive-executive mechanism that manages the precision of protein amounts: the information about the higher ECM receptor Dg levels is relayed via signalling that induces transcription of miRNAs. miRNAs can postranscriptionally regulate only a fraction of Dg mRNA with an alternative 3'-UTR, reducing the variance of the target and readjusting its levels via a negative feedback loop. We believe that this phenomenon might be indicative of a broader regulatory mechanism that could be in play to regulate ECM receptor levels in response to cell shape rearrangements in general.

Results

High levels of Dg result in cobblestone-like brain. Multiple studies imply that Dg is not only the transmembrane component of the DGC, but also is a well-designed platform that allows communication with many interacting proteins to modulate multiple cellular processes. Thus, we postulate that Dg levels need to be tightly controlled. To test this hypothesis, we used a previously established Drosophila muscular dystrophy model, where it was shown that Dg deficit leads to age-dependent muscle defects[13,16,17]. Now we tested Dg developmental requirements and found that Dg loss retards pre-adult development (Fig. 1a) and affects mutant animals' viability (Fig. 1b), while its overexpression with a ubiquitous Gal4 driver (tub-Gal4) appears to be deadly (Fig. 1c). As Dg has been shown to play important roles in muscle and nervous tissues, we wanted to dissect whether this lethality was due to the requirement for exact Dg levels in muscles or in the nervous system using different tissue-specific drivers (expression exemplified in Supplementary Fig. 1). Increasing Dg levels in the muscle did not affect viability,
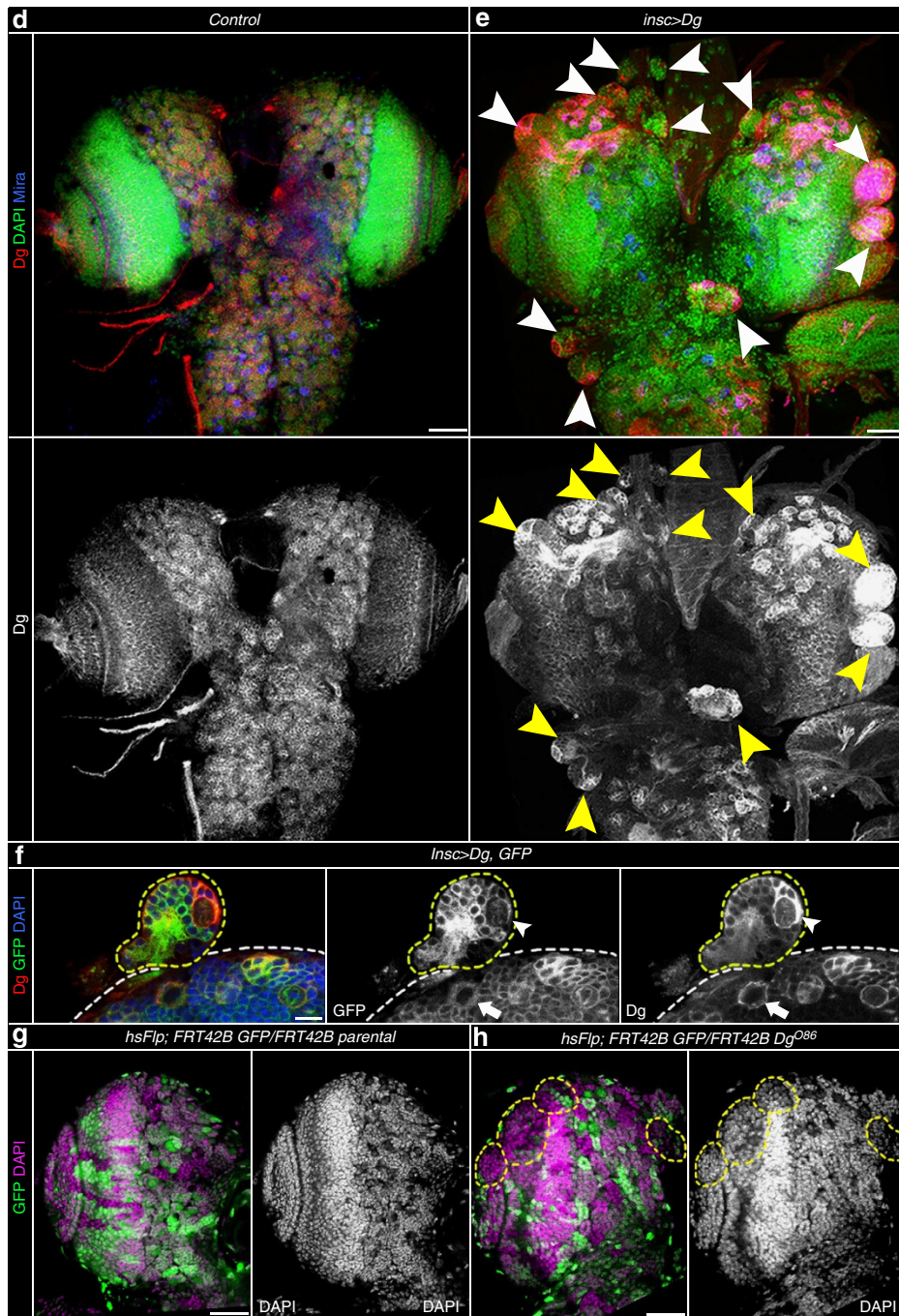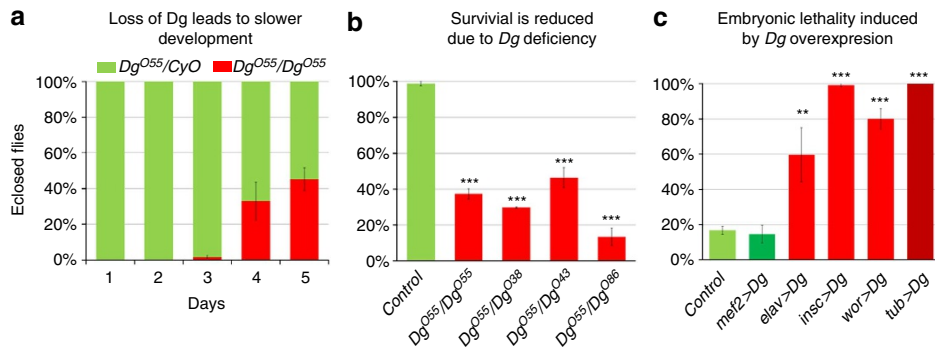
but in the nervous system caused high levels of embryonic lethality (Fig. 1c), suggesting that there might be a need to control Dg levels, specifically in the nervous system.

Next, we wanted to understand what is the cause for the lethality. Dg overexpression in the nervous system resulted in a peculiar phenotype: dense cellular masses that overgrow the normal brain contour (Fig. 1d,e; arrowheads). The majority of Dg-overexpressing mutants die during larval stages; however, a few escapers make it to adulthood. Their brains also contained lumps (Supplementary Fig. 2a–c), but in a lesser quantity than observed on average in larval brains, suggesting that the penetrance of the brain overgrowth phenotype is variable. We also noted that lump-like structures found within one brain could be irregular in size (Fig. 1e). As neuronal Gal4 drivers may have somewhat variable expression patterns, the size of the overgrowths should correlate with the localized strength of driver expression. To test this, we co-expressed green fluorescent protein (GFP) as a marker for the efficiency of Gal4 expression and full-length Dg (insc-Gal4 > UAS GFP, UAS Dg). We observed that clusters with the highest GFP levels (the strongest Gal4 activity, the highest Dg expression) produced qualitatively larger lumps (Fig. 1f), substantiating a direct correlation between the Dg amount and brain malformation. Similar effects were observed on Dg overexpression by pan-neuronal (elav-Gal4) and neuronal stem-cell-specific (wor-Gal4) drivers: some of the neuronal stem cells (neuroblasts (NBs)) expressed high, while others moderate levels of Dg (Supplementary Fig. 2d–f). Interestingly, NBs and their progeny that had similar amounts of Dg protein clustered together and grouped into separate lumps, indicating that lump size and assembly correlate with Dg levels.

To specify the time course of the abnormal lump formation and provide evidence that this effect is cell-autonomous, we took advantage of the temporally inducible FRT–FLP system to obtain Dg overexpression clonal cells. Early Dg-overexpressing clones (analysed 1 day after clone induction) did not show any obvious abnormalities; however, after 3 days, clonal cells that overexpressed Dg started to aggregate and formed clearly outlined three-dimensional masses, beginning to separate from the rest of the brain tissue (Supplementary Fig. 2g,h). Notably, induced Dg-deficient cellular clones or Dg downregulation (tub > DgRNAi) also resulted in similar brain malformations; however, the observed phenotype was milder in comparison with its overexpression (Fig. 1h and Supplementary Table 2). Thus, regardless of whether Dg levels are increased or decreased, the cobblestone-like brain phenotype appears.

These data demonstrate the following: (1) the precision of Dg expression levels affects brain morphology; (2) the severity of the observed brain defect depends on the amount and duration of abnormal Dg levels; and (3) the effect of Dg misregulation on

the brain lump formation is cell autonomous, which together implies that Dg levels must be stabilized for normal brain development.

Dg non-tumorous outgrowths caused by cell adhesion defects. Next, we wanted to understand the nature of these brain defects. First, we suspected that the observed Dg-linked brain lumps were tumours that occurred due to neuronal stem cell division and/or neuron differentiation defects. However, staining of mutant brains with the antibody against the neuronal stem cell and neuron-specific markers proved that asymmetry of neuronal stem cell division and the major differentiation processes are not affected (Fig. 2a). Thus, we concluded that these lumps were not tumours.

Second, we hypothesized that Dg's interaction with the ECM could be responsible for the cobblestone-like brain phenotype and the strength of the ECM–cell interaction could contribute to abnormal lump formation. Similar to that in vertebrates, Drosophila Dg contains two functional domains: the extracellular domain that connects to the ECM and the cytoplasmic domain that interacts with Dys and other DGC proteins[13]. To establish which functional part of Dg is responsible for the observed brain overgrowth phenotype, we overexpressed a truncated Dg version that lacks the extracellular domain (DgΔExD, Supplementary Fig. 3a). Importantly, misregulation of this version of Dg had no effect on the brain shape (Supplementary Fig. 3a–c), suggesting that the altered brain morphology due to abnormal Dg levels results from impaired Dg-ECM communication.

Therefore, we analysed the expression pattern of cell adhesion proteins in tandem with Dg overexpression. In contrast to neuronal cell differentiation markers, we found the distribution of major cell adhesion receptors and ECM molecules to be highly abnormal. According to the genotype, Dg levels were extremely upregulated in the brain outgrowths (Fig. 2b). In vertebrates, Dg is a key receptor for the major class of ECM proteins, laminins, and defects in α-Dg posttranslational modifications cause aberrant interactions with different laminins, causing muscular dystrophy development and exacerbation[22–25]. As it has not been shown that in Drosophila brain Dg interacts with laminins, we performed co-immunoprecipitation analysis with the brain-specific GFP-tagged Dg (Supplementary Fig. 3d,e) and the ECM protein LamininB (LanB), demonstrating that Dg can act as a laminin receptor in the fly brain (Supplementary Fig. 3e). Moreover, LanB was notably upregulated in the forming cysts (Fig. 2b). Another ECM protein, Perlecan (Pcan) that binds Dg in vitro[26] was also upregulated and differentially localized (Fig. 2b). LanB and Pcan are major macromolecular components of the neural lamella, the extracellular net-like

Figure 1 | Proper Dg levels are important for *Drosophila* viability and normal brain morphology. (**a**) In general, *Dg* loss-of-function animals develop slower, as adult flies eclose 3–4 days later then their heterozygous siblings. (**b**) Loss of Dg leads to decreased viability, as more than one half of Dg-deficient flies die during development (embryogenesis, larval and pupal stages). The AVE ± AD is reported. Two independent crosses for each allelic combination were analysed. Statistics were calculated using two-way tables and the χ^2-test. (**c**) Dg overexpression in the nervous system (elav > Dg, insc > Dg, wor > Dg) and ubiquitously (tub > Dg) cause high embryonic lethality. Embryos with increased muscle expression of Dg (mef > Dg) are not affected. The AVE ± s.d. is reported. Three to six biological replicates were done and the two-tailed Student's t-test was used to test for statistical significance (see also Supplementary Table 1). (**d**) In *Control*, the larval brain has a smooth outline. (**e**) Overexpression of Dg using pan-neuronal driver (insc > Dg) results in the appearance of dense rounded structures that outgrow the normal shape of the brain (arrowheads). (**f**) Dynamic expression of the nervous system driver (insc-Gal4) results in a non-uniform pattern of lump formation. Marking the expression pattern of the insc-Gal4 driver with GFP and Dg (insc-Gal4; UAS-CD8:GFP, UAS-Dg) and co-staining with anti-GFP and anti-Dg antibodies reveals that some of the NBs have low (arrow) while others have high (arrowhead) expression levels of both GFP and Dg, and that the size of lumps appears to correlate with the strength of Dg overexpression. (**g**) Parental control clones (hsFlp; FRT42B GFP/FRT42B) are marked by the absence of GFP. (**h**) Induction of Dg loss-of-function clones (hsFlp; FRT42B GFP/FRT42B Dg^{O86}) causes abnormal clustering between clonal (Dg deficient) and non-clonal (normal levels of Dg) cells, resulting in peculiar three-dimensional brain organization. This cobblestone-like phenotype occurs with the frequency ∼42% (see also Supplementary Table 2). White dashed lines indicate the normal boundary of the brain. Yellow dashed lines indicate brain outgrowths. *P ≤ 0.05, **P ≤ 0.01, ***P ≤ 0.001. Scale bar, 25 μm (**d,e,g,h**) and 10 μm (**f**).
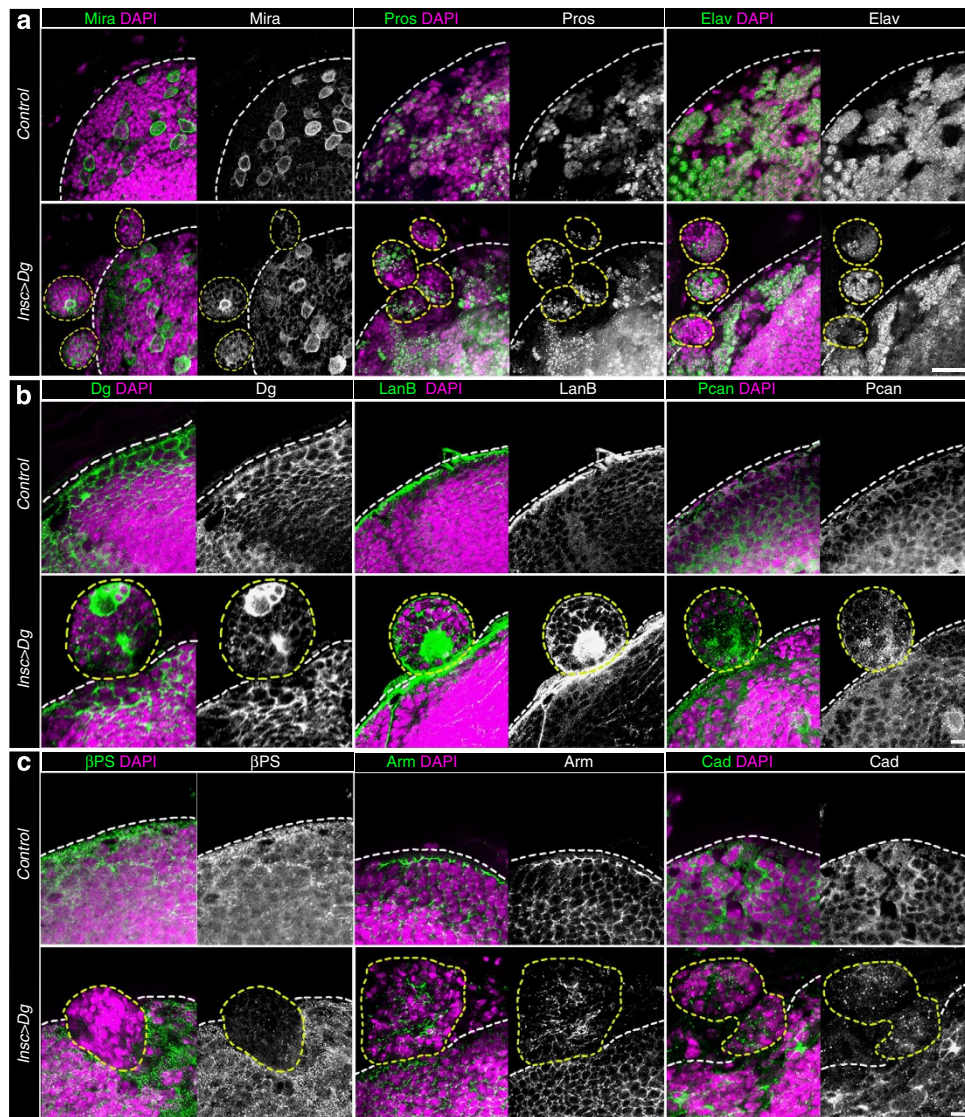
Figure 2 | Dg overexpression causes non-tumorous brain outgrowths resulting from abnormal interaction of neuronal cells with the ECM.
(**a**) Cobblestone-like malformations, which result from Dg ectopic expression in nervous system, are not tumours, as each structure contains one NB marked by the neuronal stem cell-specific marker Miranda (Mira $^+$) per cobblestone. Marking with ganglion mother cell (GMC) and neuronal markers, Prospero and Elav respectively, demonstrates typical numbers of GMCs marked with Prospero (Pros $^+$) and differentiated neurons (Elav $^+$), when compared with *Control*, indicating that asymmetry of neuronal stem cell division and major differentiation processes are not affected. (**b**) Overexpression of Dg influences the distribution of cell adhesion proteins: the transmembrane ECM receptor Dg, the ECM proteins LanB, Pcan; heterophilic cell adhesion protein β-integrin (β-PS), the β-Catenin homologue Armadillo (Arm) and homophilic cell adhesion protein DE-Cadherin (Cad), when compared with *Control*, suggesting that the above described malformed brain phenotype results from abnormal interaction of neuronal cells with the ECM. White dashed lines indicate the normal boundary of the brain. Yellow dashed lines indicate brain outgrowths. Scale bar, 20 μm (**a**) and 10 μm (**b,c**).

ECM sheet that outlines the developing brain. On Dg misregulation, lumps protrude above this ECM-formed outermost brain layer (Fig. 2b). At the same time, levels of the major extracellular receptor required for cell–ECM interaction, integrin (βPS), is drastically reduced in these structures compared with *Control* (Fig. 2c). It is known that Dg competes with integrins for ECM binding, and levels of both Dg and integrins are co-dependently readjusted at the transcriptional level via the ECM[27]. Thus, Dg misregulation alters the βPS integrin expression pattern and ECM composition, such as LanB and Pcan levels and distribution. In addition, higher Dg levels cause reduction as well as mislocalization of cell–cell adhesion proteins at the cellular membrane (β-catenin = Arm and E-cadherin = Cad, Fig. 2c). Together, these data demonstrate that the Dg-malformed brain

phenotype is associated with abnormal cell–ECM and cell–cell adhesion.

Thus, on Dg misregulation, neuronal cells express altered levels of ECM molecules and cell adhesion receptors, which cause abnormal interaction of these cells with the rest of the brain tissue. As a result of selective cell adhesion, these cells with aberrant Dg levels cluster together, forming lumps that are dissociated from other cells and are pushed out from the brain. Notably, similar cobblestone brain structure is a characteristic of lissencephaly type II in humans suffering from dystroglycano-pathies[10,28], which are also caused by abnormal α-Dg interaction with the ECM. Resemblance of the brain phenotypes proposes that *Drosophila* Dg mutants can be used as a model to study these neurodevelopmental diseases.

Dg can be accessible to miRNA regulation via a variable 3'-UTR. Owing to the evidence that Dg needs to be precisely regulated in the nervous system, we next studied the mechanism of how Dg can be regulated there. The *Dg* transcript has the possibility of having at least two different *3'-UTRs* according to *FlyBase* annotation (Fig. 3a). Recently, it has been shown that *3'-UTRs* of metazoan mRNAs contain various regulatory motifs that influence mRNA stability, localization and translational efficiency, affecting numerous cellular processes[29,30]. It is logical to hypothesize that longer *3'-UTRs* may contain regulatory motifs that can be used to fine-tune spatiotemporal signalling. When we probed Dg complementary DNA with primers that recognize a region belonging to both the short and long *3'-UTR* and a region of only the long *3'-UTR*, we found that ~60% of *Dg* transcripts have the longer *3'-UTR* version (Fig. 3b). mRNA *in situ* hybridization using a probe with primers that recognize the

long *3'-UTR* showed expression in the brain, imaginal disks, muscles and other tissues (Fig. 3c and Supplementary Fig. 4a) and no obvious difference in expression patterns was observed between the Dg protein[13,14,16] and the *Dg* long *3'-UTR* mRNA.

As *Dg* has an alternative *3'-UTR*, it can be reasoned that there is a regulatory function for this diversity. Theoretically, by varying the *3'-UTR* length, *Dg* becomes more or less visible to regulation by miRNAs. For example, the short *3'-UTR* does not have, while the Dg-extended *3'-UTR* has, a predicted binding site for a family of miRNAs, the *miR-310s* (*miR-310, miR-311, miR-312, miR-313*), *miR-92a* and *miR-92b*, which we found to be Dg-dependent in our miRNA microarray screen[19]. The long *3'-UTR* is evolutionarily conserved and present among all *Drosophila* species, but the conservation in the sequence corresponding to the seed of the newly evolved *miR-310s* miRNA family (Fig. 3a) developed along with the emergence of the *miR-310s*, via *miR-92a/b* duplication, around 53 million years ago[31]. As the conservation of the corresponding sequence necessary for targeting by the *miR-310s* appeared at the same time as these miRNAs emerged, we thought that it might be physiologically relevant and, next, we examined whether the *miR-310s* can target Dg.

First, to determine whether the *miR-310s* target Dg's extended *3'-UTR*, we assayed a luciferase reporter gene with different *3'-UTR* fragments in *Drosophila* S2R+ cells (Supplementary Table 3). The luciferase assay showed that the *miR-310s* can target Dg via the extended *3'-UTR in vitro* and confirmed the *miR-310* seed sequence specificity (Fig. 3d). Next, we also verified that *Dg* could be targeted by the *miR-310s* in *Drosophila* tissue, where we analysed ovarian follicle cell clones that ectopically express the *miR-310s* (Supplementary Fig. 4c). Together, these data demonstrate that the *miR-310s* can downregulate Dg *in vitro* and *in vivo* via its long *3'-UTR*. Finally, we tested whether *miR-310s*-based
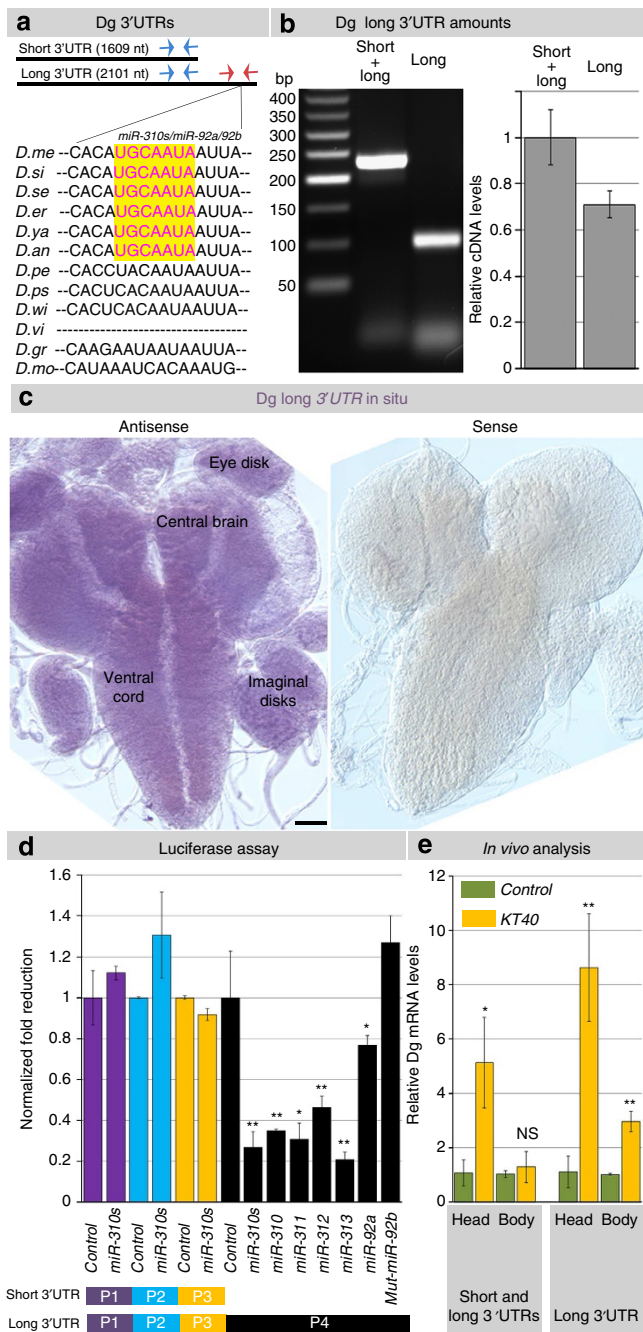

Figure 3 | *Dg's* variable *3'-UTR* allows for alternative targeting by *miR-310s*. (**a**) Schematic drawing of the variable Dg *3'-UTRs*, the short and the long that is extended by an additional 491 bp. Arrows mark the location of primers used to detect *Dg* mRNA with both the shorter and the long *3'-UTR*, and just the long *3'-UTR*. (**b**) PCR analysis of cDNA from whole flies with primers that recognize the region of the long *3'-UTR*, and the region common for both long and short *3'-UTR* versions of *Dg* transcript show that ~60% of the *Dg* mRNA has the longer *3'-UTR* region present (analysis was done taking into the account primer efficiencies). (**c**) *In situ* hybridization against the long *3'-UTR* region shows that the long *3'-UTR* containing *Dg* mRNA is present in the larval brain. Scale bar, 25 μm. (**d**) Consistent with the fact that only the extended version of the *Dg 3'-UTR* has the *miR-310s* binding site, no reduction in luciferase activity is observed when fragments of the *Dg 3'-UTR* common for the short and long *Dg 3'-UTRs* (but without the *miR-310s* binding site) were assayed (P1, P2 and P3). When the reporter gene fused to an appropriate fragment of the *Dg* long *3'-UTR* containing the *miR-310s* putative binding site is assayed (P4), a decrease in luciferase activity is observed even in the absence of miRNA transgenes (~1.5-fold), presumably due to endogenous levels of targeting miRNAs in the cells. When also transformed with plasmids expressing *miR-310s* (all), individual cluster miRNAs and *miR-92a* (but not *mut-miR-92b* that contains a single point mutation in the seed sequence, CACTGCA instead of CATTGCA), a further decrease in luciferase activity (~1.3- to 4.7-fold) is seen (Supplementary Table 3). (**e**) KT40 mutants (loss of *miR-310s*) have elevated levels of total *Dg* mRNA detected by primers that recognize both short and long *3'-UTRs*. This upregulation is more pronounced when primers specifically against the long *3'-UTR* region or RNA extracts from heads were used (Supplementary Table 4). Three to five independent biological experiments were analysed. The AVE ± s.d. is reported and two-tailed Student's *t*-test was used to test for statistical analyses: *$P \leq 0.05$, **$P \leq 0.01$, ***$P \leq 0.001$, NS, not significant.
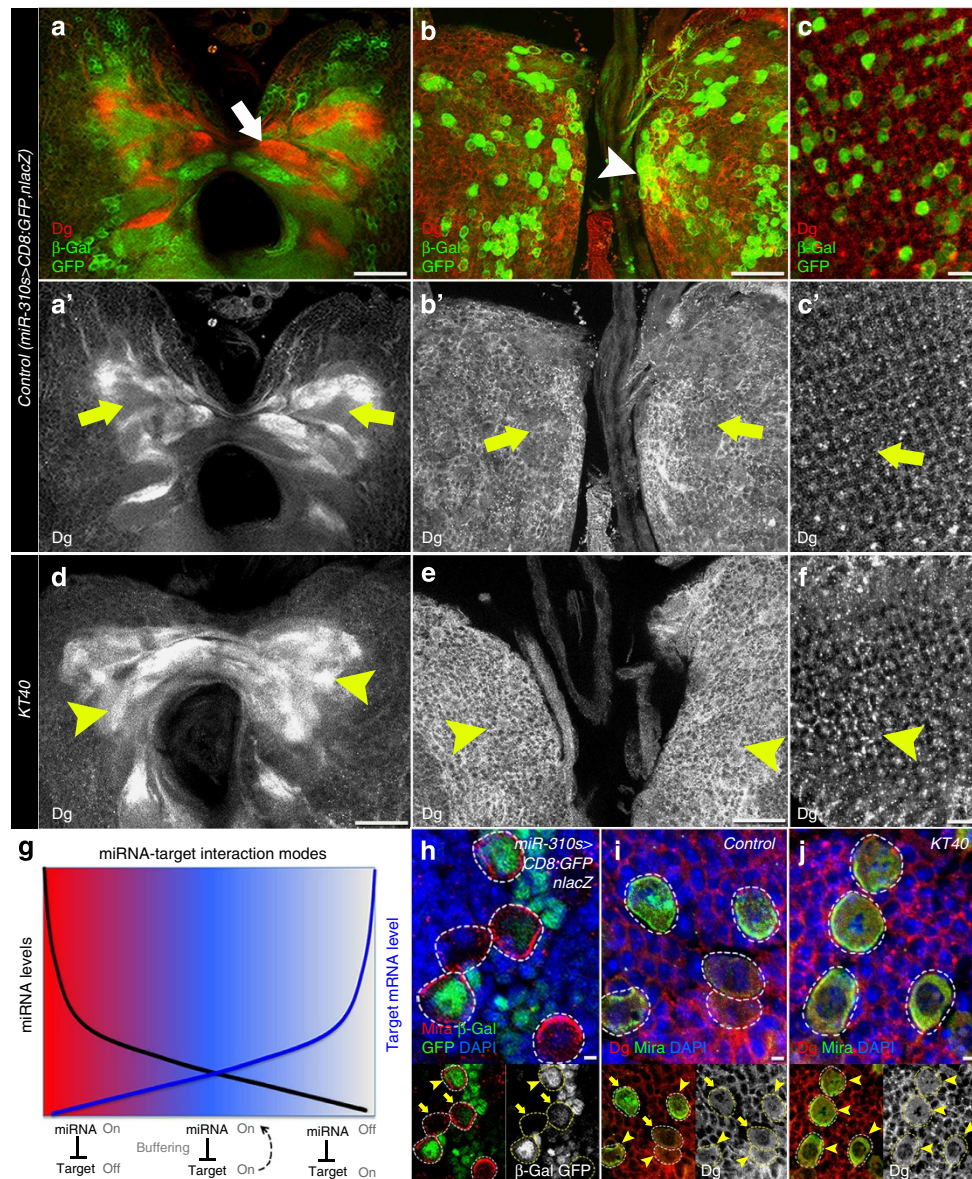
Figure 4 | Complementary and non-complementary expression of *Dg* and *miR-310s*. (**a–c**) Analysis of the expression patterns of Dg protein and the *miR-310s* revealed that there are two possible modes of how *miR-310s* can regulate Dg levels. Axonal bundles in the central brain neuropils express Dg and *miR-310s* in a mutually exclusive pattern (**a**), meaning that there is no regulation or that a miRNA completely downregulates its target. Cells located at the brain surface express both, the *miR-310s* and Dg (**b**), meaning that a miRNA buffers its target levels. A similar co-expression pattern is observed in the visual system (**c**). As a readout of *miR-310s* expression, we used a Gal4 insertion in the *miR-310s* locus, *P(GawB)NP4255* (referred to as *miR-310s-Gal4*) from Kyoto DGRC. *miR-310s* expression was visualized by anti-β-Gal and anti-GFP antibodies in the brain expressing nuclear lacZ and membrane GFP under control of the *miR-310s* promoter (*miR-310s-Gal4/ + ; UAS-mCD8-GFP, UAS-nLacZ/ +*). Dg was visualized by antibody staining. (**d–f**). To test how the *miR-310s* regulate Dg in the brain, we analysed Dg expression in *KT40* mutants. In *miR-310s* mutants, the Dg expression pattern is altered in the central brain region (**d**), more axonal bundles expressed Dg in the absence of *miR-310s*, confirming the idea that *miR-310s* and Dg are expressed in the 'off/on' mode in the central brain axons. Similarly, Dg expression levels are increased in the brain surface neuronal and photoreceptor cells (**e,f**) in comparison with Control (**a',b'** and **c'**), suggesting that the *miR-310s* also buffer Dg levels. (**g**) Scheme representing the architecture of the miRNA-target network: expression tuning and expression buffering (modified from ref. 33). (**h**) Neuronal cells express the *miR-310s* in a selective manner (arrows and arrowheads). (**i,j**) Dg is expressed in all of the cells of the larval brain with somewhat variable levels (arrows and arrowheads). Dg expression levels are increased in all neuronal cells in the larval brain of *miR-310s* mutant (**j**, arrowheads). White dashed lines outline NBs in **h–j**. Scale bar, 25 μm (**a,b,d,e**), 5 μm (**c,f**), 2 μm (**h–j**).

regulation of Dg has a functional role in living animals. We found that *miR-310s* loss-of-function mutants, *KT40* (ref. 32) have higher levels of total *Dg* mRNA detected by primers that recognize the short and long *3'-UTRs* and only the long *3'-UTR* (Fig. 3e). This dramatic increase in Dg expression could be also seen at the protein level measured by western blot analysis (Supplementary Fig. 4b). *Dg* mRNA levels were increased even

more in heads alone, indicating that Dg regulation is primarily occurring in the head. Moreover, *Dg* mRNA levels with the long *3'-UTR* in the head increased ~8.5 times, presumably due to Dg targeting in the central brain and eyes (Fig. 3e). The determining mechanism for transcribed *3'-UTR* length is ambiguous, but in the presence of mixed *3'-UTRs* certain levels of Dg would be maintained via invisibility to *miR-310s* targeting, offering

protection from Dg deficit. We next sought to define whether Dg and the *miR-310s* have similar expression in the nervous system and whether they share other phenotypes.

miR-310s and Dg expression in the nervous system is dynamic. We analysed the expression pattern of Dg and the *miR-310s*. Interestingly, we found that there are two possible modes of how *miR-310s* can regulate Dg levels: axonal bundles in the central brain neuropils express Dg and *miR-310s* in a mutually exclusive pattern (Fig. 4a–a′), while cells located at the brain surface or in the developing visual system express both the miRNA and its target Dg (Fig. 4b–c′). miRNA functions can be classified into two categories: expression tuning (when a miRNA is setting the mean of the expression level of the target gene resulting in the 'on-off' expression pattern) and expression buffering (when a miRNA reduces the variance of the target where the miRNA and its target are co-expressed). These two functions are independent and can co-exist (Fig. 4g, reviewed in ref. 33). Dg protein expression analysis in *miR-310s* deficient flies shows that *miR-310s* and Dg could interact in the expression tuning and buffering modes (Fig. 4d–f).

Dg, detected by antibody staining, is broadly expressed in the nervous system and, as expected, its levels are variable. For example, some neuronal stem cells had higher, while others had lower or undetectable, Dg amounts (Fig. 4i). The fluctuating Dg levels were also characteristic for other cells in the brain, suggesting that its levels vary, possibly during different stages of the neuronal lifecycle, such as cell division or neuron maturation. We analysed in detail neuronal cells that co-express Dg and the *miR-310s*. If Dg levels fluctuate, they must be re-adjusted; therefore, we analysed in more detail neuronal cells that co-express Dg and the *miR-310s*. *miR-310s* expression (marked by nuclear lacZ, *miR-310s>nlacZ*, driven by the endogenous *miR-310s* promoter) was detected in a subset of each Dg-expressing cell type on the brain surface and their expression levels were also fluctuating (Fig. 4h and Supplementary Fig. 5a). However, on *miR-310s* loss, Dg levels were visibly increased in all brain cells (Fig. 4i,j). Comparison of the expression patterns shows that Dg and the *miR-310s* are expressed in some of the same cell types and their levels are dynamic, confirming the expression-buffering mode of *miR-310s*-Dg interaction (Fig. 4g).

Considering that Dg levels are critical for proper formation of the nervous tissue and that the *miR-310s* can regulate only isoforms of the Dg mRNA with the extended *3′-UTR* (~60% of total Dg mRNA), we propose that the *miR-310s* buffer the expression of its target Dg against fluctuation, perhaps dynamically.

Dg and miR-310s fine-tune the mitotic index of neuronal stem cells. As miRNA-based regulation could offer additional safeguarding, we next investigated the biological significance of Dg buffering by these miRNAs in the nervous system. We tested whether similar phenotypes are associated with *Dg* deregulation and the *miR-310s* loss in the developing brain. Importantly, we found that the *miR-310s* loss-of-function mutant, similar to *Dg* loss- and gain-of- function mutants, exhibits cobblestone brain (Supplementary Table 2), suggesting that Dg buffering by the *miR-310s* via Dg's extended *3′-UTR* is relevant for brain development.

Dg misregulation affects the amounts of multiple proteins involved in cell adhesion (Fig. 2c), intensity of which modifies multiple aspects of the cellular lifecycle, including cell proliferation[6,34]. In particular, we found that the loss of Dg results in a decreased number of mitotically active neuronal stem cells, NBs (Fig. 5a–d). Moreover, Dg overexpression in *miR-310s*-expressing cells and *miR-310s* deficiency caused a significant over-

proliferation rate, while Dg deficit substantially decreased the NB mitotic index (Fig. 5d). These data show that managing the levels of *miR-310s* and the ECM receptor Dg is important to fine-tune the mitotic index of neuronal stem cells. We hypothesize that this is because NB cell divisions are normally accompanied by cell–ECM and cell–cell contact rearrangements requiring a proper ECM composition that depends on Dg amounts.

miR-310s regulation of Dg is necessary in the visual system. Other processes, accuracy of which highly depends on ECM composition, are neuron differentiation and axon pathfinding. Therefore, next we analysed whether the miRNA-based regulation of Dg levels takes place in the visual system, where Dg previously has been shown to play an essential role in terminal differentiation of *Drosophila* photoreceptor neurons[13,16]. We found that only some of the photoreceptor neurons within ommatidium express the *miR-310s* and that Dg levels are *miR-310s* dependent; in *miR-310s* mutants, Dg was accumulated and its cellular localization was affected in these cells (Fig. 6a–c and Supplementary Fig. 5).

Photoreceptor neurons undergo complex reorganization during development: migration, axon growth and projection, and synapse formation, and all of these events are associated with dynamic cell shape rearrangements that are highly dependent on cell adhesion (reviewed in ref. 1). Ectopic *Dg* expression in photoreceptor neurons and specifically in *miR-310s*-expressing cells recapitulates the premature axon stops noted in *miR-310s* mutants (Fig. 6d–h). Importantly, reduction of Dg specifically in photoreceptor cells and *miR-310s* overexpression can rescue the premature axon termination phenotype in the *miR-310s* mutant background (Fig. 6h), showing that regulation of exact Dg levels via the *miR-310s* is important for proper photoreceptor neuron differentiation.

In summary, these data show that in the nervous system maintaining precise levels of the ECM receptor, Dg, is particularly important, as Dg abnormal levels affect distribution of cell adhesion proteins, subsequently influencing neuronal stem cell division speed, neuron differentiation and nervous tissue morphology.

Dg regulates miR-310s expression via a negative feedback loop. If the *miR-310s* are assigned to buffer Dg only when required, it is possible that miRNA expression itself could be sensitive to higher levels of the target. Thus, we hypothesize that the *miR-310s* promoter can be responsive to Dg amounts, which would reassure homeostatic Dg levels. To confer the responsiveness of *miR-310s* expression to abnormal Dg levels, we overexpressed *Dg* with the dynamic *miR-310s* promoter that is shared by all miRNAs in the *miR-310s* family and measured the levels of a representative miRNA, *miR-312*. We observed an ~5-fold increase in *miR-312* levels due to Dg overexpression, reciprocally, Dg loss results in lower levels of *miR-312* (Fig. 7a). This effect can also be visualized on the cellular level; for example, when in *Control*, the majority of ommatidia in the eye imaginal disk contain two cells that have the transcriptionally active *miR-310s* promoter, and *Dg* overexpression results in more cells actively expressing the *miR-310s* (Fig. 7b,c). These data imply that the *miR-310s* and Dg are in a negative feedback loop, where expression of miRNAs is induced in response to higher levels of their target (Fig. 7d).

Dg regulates miR-310s expression via NO signalling. Dg is a transmembrane receptor and the question of how it can regulate *miR-310s* expression at the transcriptional level needs to be answered. Previously, it has been shown in vertebrates that the DGC acts as a scaffold responsible for the membrane localization
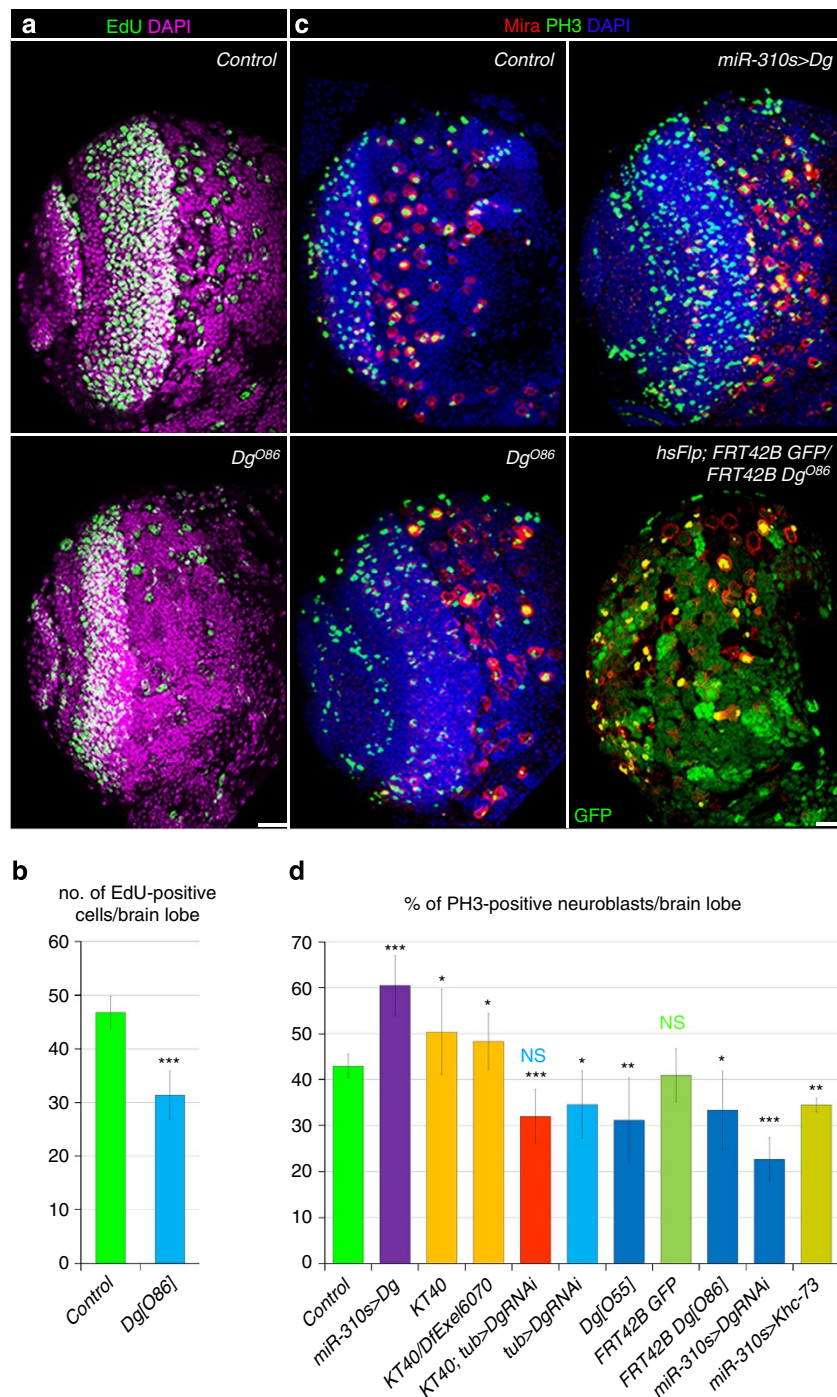
Figure 5 | The *miR-310s* and Dg regulate proliferation of neuronal stem cells. (a,b) On Dg deficiency, the frequency of actively dividing cells (S phase, marked by EdU) is significantly decreased in the larval brain in comparison with *Control*. Fourteen to 16 lobes were counted per genotype. **(c,d)** On Dg deficiency (Dg^{O86}, Dg^{O55} and FRT42B Dg^{O86} clones) or Dg downregulation using RNAi driven by the ubiquitous and the dynamic *miR-310 Gal4* drivers (*tub > DgRNAi* and *miR-310s > DgRNAi*), the frequencies of NBs in M phase (marked by PH3 and Mira, yellow) are significantly decreased. *Dg* overexpression in *miR-310s*-expressing cells results in overproliferation defects comparable to the defects occurring due to the loss of the *miR-310s* (*KT40* and *KT40/DfExel6070*), the mitotic index of larval brain NBs significantly increased compared with *Control*. Six to 17 lobes were counted per genotype. To prove that this decrease in the number of PH3- and EdU-positive NBs is not due to increased apoptosis induced by the absence of the principal ECM receptor, activated Caspase3 staining was performed in Dg loss-of-function (Dg^{O55}) mutants and no elevated numbers of apoptotic cells per brain were observed; four out of nine brains had one apoptotic cell where the maximum number of positive cells seen was four in one brain, which was similar to *Control*. Dg knockdown cannot rescue the *miR-310s* deletion phenotype (compare *KT40; tub > DgRNAi* and *tub > DgRNAi*), plausibly because RNAi-based downregulation of Dg is more efficient than Dg upregulation resulting from *miR-310s* loss. Overexpression of another confirmed *miR-310s* target, Khc-73 (ref. 32) (*miR-310s-Gal4/UAS-Khc-73*), decreases the mitotic index, which is opposite to the increase seen in *KT40* and *miR-310s-Gal4/UAS-Dg* mutants. These data confirm previous findings about the role for Khc-73 in NB division; however, this shows that the increased proliferation phenotype observed in *miR-310s* loss-of-function mutants is not due to an *miR-310s-Khc-73* interaction in NBs. See also Supplementary Table 5. The AVE ± s.d. are reported and significance was tested using the two-tailed Student's *t*-test: *$P \leq 0.05$, **$P \leq 0.01$, ***$P \leq 0.001$, NS, not significant. Scale bar, 25 μm.
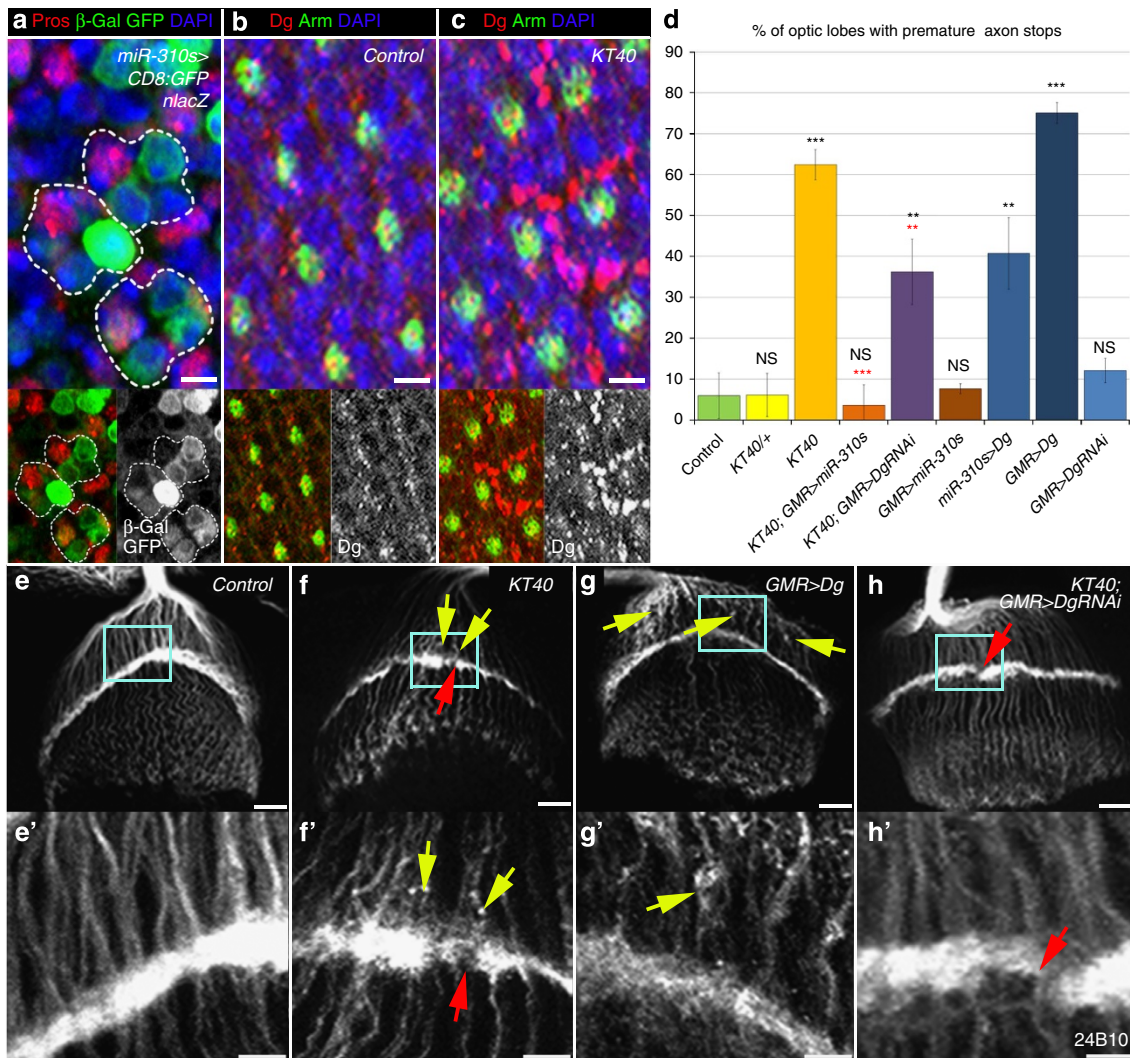
Figure 6 | Dg regulation by the *miR-310s* is important for proper photoreceptor axon guidance during development of the visual system. (a) The *Drosophila* compound eye consists of ∼800 ommatidia that each contains 8 photoreceptor neurons or R-cells (R1–8). The *miR-310s* are expressed variably in photoreceptor neurons visualized with anti-β-Gal and anti-GFP (*miR-310s-Gal4/+; UAS-mCD8-GFP, UAS-nLacZ/+*), and the R7 marker Prospero (Pros)[57] (white dashed lines outline a single ommatidium). Note that nuclear β-Gal and membrane GFP do not always co-localize: β-Gal and GFP have different protein turnover rates, suggesting dynamic *miR-310s* expression. **(b)** Dg is expressed in all photoreceptor neurons. **(c)** Dg levels are *miR-310s* dependent; in *KT40* photoreceptor cells, Dg is accumulated and its cellular localization is affected. However, due to the nature of the used reporter that visualizes *miR-310s* expression via lacZ and GFP proteins, which depends on the time of their production and degradation, it is not feasible to evaluate the corresponding *miR-310s* and Dg protein levels in a given cell. See also Supplementary Fig. 5b. **(d)** The bar graph represents percentages of defective axon projections in the indicated genotypes. The experiment was conducted using three different bouts of progeny from independent crosses (biological replicate). Each experimental round consisted of between 5 and 20 optic lobe examinations being marked as disturbed or normal to generate an experimental percentage per biological replicate. The AVE ± s.d. is reported and the two-tailed Student's *t*-test was used to test for statistical significance: *$P \leq 0.05$, **$P \leq 0.01$, ***$P \leq 0.001$, NS, not significant. Black stars—compared with *Control* (*w^1118*), red stars—compared with *KT40* mutants. See Supplementary Table 6. **(e,f)** In contrast to *Control* (**d**), in the *KT40* mutants (**e**) axon terminations in the lamina plexus have gaps and breaks (red arrows), reminiscent of the photoreceptor axon pathfinding defects in *Dg* loss-of-function mutants, but additionally mutants have premature axon stops (yellow arrows). **(g)** Ectopic expression of *Dg* using *miR-310s-Gal4* and *GMR-Gal4* drivers recapitulates the premature axon stops noted in *KT40* mutants only. **(h)** The premature termination phenotype and lamina plexus gaps can be rescued in *KT40* mutants by overexpressing the *miR-310s* (*KT40; GMR>miR-310s*; Supplementary Table 6). Accordingly, premature axon termination can be rescued by reduction of Dg (*KT40; GMR>DgRNAi*) in the eye. **e'–h'** are enlarged regions outlined in cyan in **e–h**. Scale bar, 2 µm (**a–c**), 10 µm (**e–h**) and 5 µm (**e'–h'**).

of signalling proteins (Fig. 8a). In particular, Dg, via Dys or Dystrobrevin, anchors Syntrophins (Syn) that bind neuronal NO synthase and, as a result, regulate generation of NO[35,36]. NO nitrosylates the histone deacetylases that regulate gene transcription and in vertebrate muscles the Dys-Syn-neuronal NO synthase signalling pathway regulates histone modifications that control transcription of miRNA genes[37]. Recently, we showed that in *Drosophila*, Dg-Dys-Syn signalling also controls

the miRNA expression profile[19]. Therefore, we decided to test whether Dg-mediated regulation of *miR-310s* expression occurs via NO signalling.

First, we addressed whether the outgrowth phenotype induced by Dg overexpression depends on the DGC being a platform for NO signalling. To test this, we analysed Dys expression in the mutant brains and found that on Dg overexpression Dys amounts at the protein (but not mRNA) levels are significantly increased
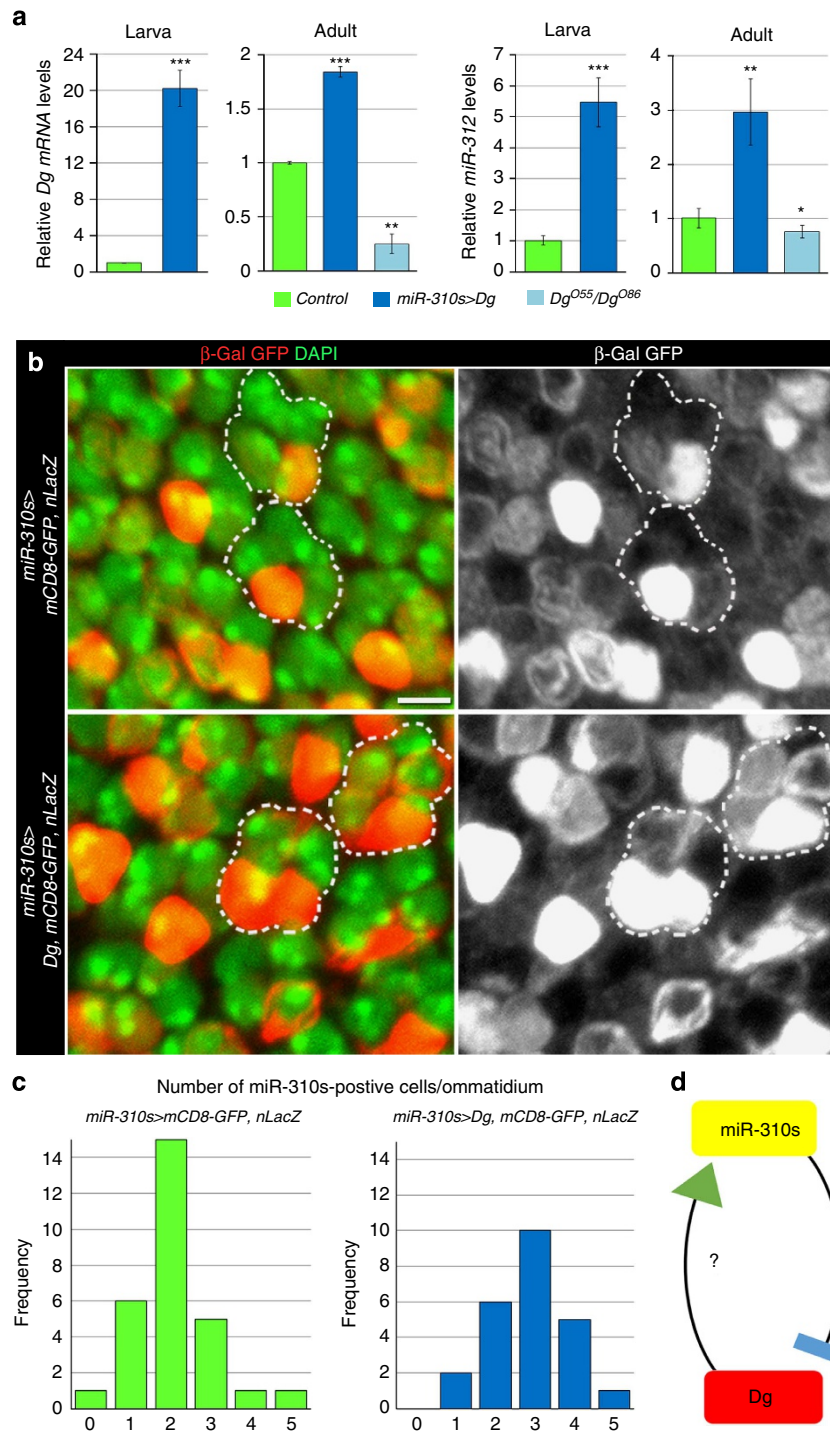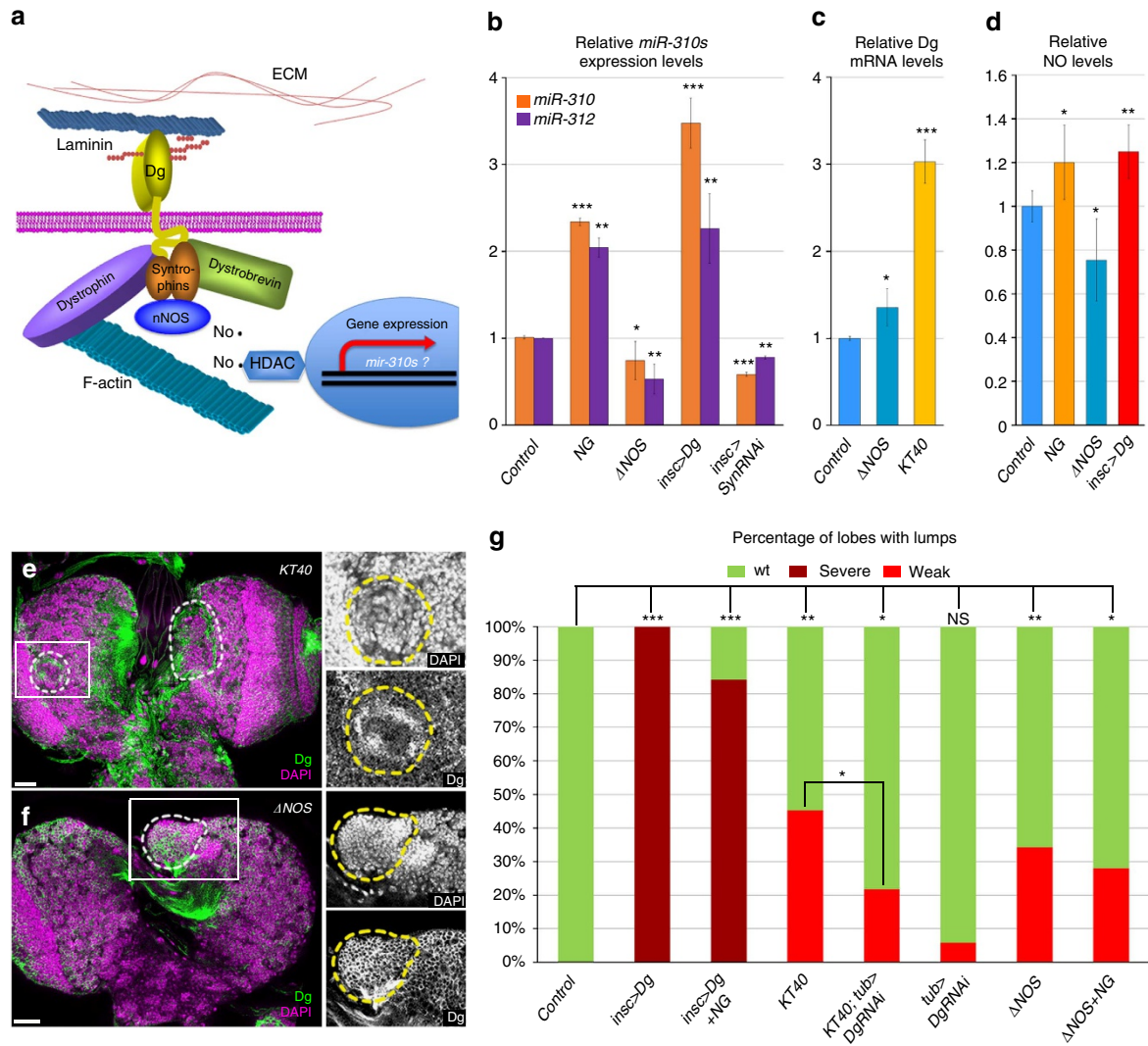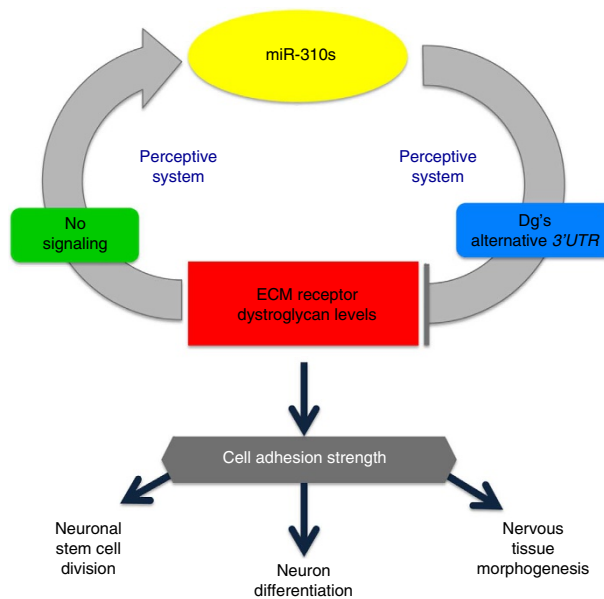
Figure 7 | *miR-310s* expression depends on Dg levels. (**a**) *Dg* mRNA levels are upregulated in flies where Dg is expressed under control of the *miR-310s* endogenous promoter. High levels of Dg coincide with increased, while lack of Dg with decreased amounts of *miR-312*, one of the miRNAs from the *miR-310s* complex. Three independent biological replicates were analysed. The AVE ± s.d. is reported and the two-tailed Student's *t*-test was used to test for statistical significance: *$P \leq 0.05$, **$P \leq 0.01$, ***$P \leq 0.001$. See Supplementary Table 4. (**b**) Dg overexpression (*miR-310s-Gal4/ +; UAS-Dg/UAS-mCD8-GFP, UAS-nLacZ*) in *miR-310s*-expressing cells marked by anti-GFP and β-Gal staining leads to an increased number of cells positive for GFP and β-Gal in comparison with animals that do not overexpress *Dg* (*miR-310s-Gal4/ +; UAS-mCD8-GFP, UAS-nLacZ*). Scale bar, 2 μm. (**c**) Histogram showing the frequency of *miR-310s*-positive cells/ommatidium (*miR-310s-Gal4/ +; UAS-mCD8-GFP, UAS-LacZ, n = 29* ommatidia, *miR-310s-Gal4/ +; UAS-Dg/UAS-mCD8-GFP, UAS-nLacZ, n = 24*). The two-tailed Mann–Whitney U-test predicts statistical significance with $P = 0.0027$. (**d**) Schematic model showing the *miR-310s* and Dg regulation in a negative feedback loop.

(Supplementary Fig. 6). Plausibly, Dys is stabilized when bound to Dg and it is anchored to the membrane. The increase of both major components of the complex, specifically in brain lumps, allows the assumption that the outgrowth phenotype induced by overexpression of Dg does occur through the DGC. Next, we tested whether the levels of *miR-310s* expression depend on DGC-NO signalling. To provide the mechanistic evidence for NO regulation of *miR-310s*-Dg expression, we fed *Drosophila*

Figure a: Diagram showing ECM, Laminin, Dg, Dystrophin, Syntrophins, Dystrobrevin, nNOS, F-actin, HDAC, and Gene expression (mir-310s?).

Figure b: Relative miR-310s expression levels. Legend: miR-310 (orange), miR-312 (purple). X-axis: Control, NG, ΔNOS, insc>Dg, insc>SynRNAi.

Figure c: Relative Dg mRNA levels. X-axis: Control, ΔNOS, KT40.

Figure d: Relative NO levels. X-axis: Control, NG, ΔNOS, insc>Dg.

Figure e: KT40. Dg (green), DAPI (magenta); insets DAPI and Dg.

Figure f: ΔNOS. Dg (green), DAPI (magenta); insets DAPI and Dg.

Figure g: Percentage of lobes with lumps. Legend: wt (green), Severe (dark red), Weak (red). X-axis: Control, insc>Dg, insc>Dg +NG, KT40, KT40;tub>DgRNAi, tub>DgRNAi, ΔNOS, ΔNOS+NG.

Figure h: Model for perceptive-executive mechanism of miRNA-based Dystroglycan buffering. miR-310s; Perceptive system; No signaling; Dg's alternative 3'UTR; ECM receptor dystroglycan levels; Cell adhesion strength; Neuronal stem cell division; Neuron differentiation; Nervous tissue morphogenesis.

nitroglycerin (NG) as a NO donor and measured the levels of *miR-310* and *miR-312*. Importantly, NG treatment significantly increased, while NO synthase deficiency[38] (*ΔNOS*) or Syn downregulation in the nervous system (*insc>SynRNAi*)

significantly decreased these miRNAs levels, conferring the *miR-310s* promoter responsiveness to NO signalling (Fig. 8b). Even more, similar to *miR-310s* mutants, Dg levels were upregulated on NO synthase deficiency (Fig. 8c).

Table 1 | *3′-UTRs* of known *Drosophila* ECM receptors.

Gene name	Binding partners	Extended 3′-UTR variants	miRNA binding sites in extended regions of 3′-UTR (TargetScan)[58]	Nervous system phenotypes
		Non-integrin ECM receptors		
Dystroglycan (Dg)	Laminin, Perlecan	1,609–2,100 nt	miR-315 miR-33 miR-985 miR-927 *miR-310s*/92a,b miR-964 miR-iab4as*	NMJ defects, reduced number of synaptic boutons
division abnormally delayed (dally)	Hedgehog, Decapentaplegic, Magu	834–1,873 nt	n/a	Cell cycle defects of lamina precursors
Syndecan (Sdc)	Slit, Robo, Nrx IV, Laminin A, DLAR	335–945 nt 945–1,956 nt	miR-989 mir-281-2-5p miR-967* n/a	Pathfinding errors in CNS midline, retinal and motoraxons
dally-like protein (dlp)	Wingless, Hedgehog, Branchless	none	—	Misrouted CNS midline and retinal axons
		Integrin ECM receptors		
multiple edematous wings (mew, αPS1 integrin)	Laminin A, Slit	160–460 nt	miR-932 miR-961	Misguided motor nerves
		460–1,207 nt	miR-285/995/998 miR-1013 miR-1007 miR-993 miR-34 miR-1002 miR-252 miR-956 miR-929 miR-8 miR-976 miR-987* miR-961* miR-315* miR-964* miR-927* miR-1003/1004*	
inflated (if, αPS2 integrin)	Laminin W, Slit, Tenectin, Thrombospondin	None	—	Misguided motor nerves, errors in CNS pathfinding
scab (αPS3 integrin)	Laminin W, Slit	None	—	Errors in CNS pathfinding, learning defects
αPS4	ND	None	—	ND
αPS5	ND	None	—	ND
myospheroid (myo, βPS integrin)	αPS1-5	None	—	Misguided motor nerves, errors in CNS pathfinding, NMJ defects
βint-v (βv integrin)	ND	None	—	ND

CNS, central nervous system; ECM, extracellular matrix; NMJ, neuromuscular junction; n/a, extended 3′-UTR sequence is not present; ND, not determined; UTR, untranslated region.
*Non-conserved miRNA binding site (*D. melanogaster* specific)

Figure 8 | *miR-310s* gene expression depends on Dg and NO signalling to adjust Dg via a feedback loop. (**a**) Schematic drawing represents the DGC and its potential role in regulating *miR-310s* through NO signalling. (**b**) *miR-310* and *miR-312* levels are increased on treatment of wild-type larvae with the NO donor, NG and are decreased in *ΔNOS* and *insc>SynRNAi* mutants. (**c**) *Dg* mRNA levels are increased in *ΔNOS* and *KT40* larvae (Supplementary Table 4). (**d**) NG treatment, similar to Dg overexpression (*insc>Dg*), leads to significantly higher NO levels, while in *ΔNOS* mutants relative NO levels are significantly decreased. See Supplementary Table 7. (**e,f**) Similar to Dg overexpression, brains with lumps that have high levels of Dg can be observed in *KT40* (**d**) and *ΔNOS* (**e**) mutants. Note that the observed cobblestone phenotype is milder than in Dg-overexpressing flies. Scale bar, 25 μm. (**g**) Bar graph represents percentages of brain lobes that contain lumps in the indicated genotypes. The observed mutant phenotype can be rescued in *KT40* mutants by downregulation of Dg with ubiquitous driver (*KT40; tub>DgRNAi*). See Supplementary Table 2. (**h**) Schematic model showing that dynamic expression of *miR-310s* in the nervous system can be regulated by Dg and NO signalling via a negative feedback loop. Three to six biological replicates (**b–d**) and 16–108 brain lobes from 3 to 5 independent biological experiments (**g**) were analysed. The AVE ± s.d. is reported. To calculate the statistical significance the two-tailed Student's *t*-test was used in **b** and **c**, two sample *z*-test in **d** and two-way tables and the χ^2-test in **g**: *$P \leq 0.05$, **$P \leq 0.01$, ***$P \leq 0.001$.

As Dg is an anchor protein required for localization of NO signalling components, its amounts potentially can regulate NO signalling strength and play an indirect role in control of at least miR-310s expression. Therefore, we tested NO levels in flies that overexpress Dg in the nervous system and observed that relative NO levels were increased, which was comparable to the amounts measured on NG treatment, while in NOS-deficient flies these were significantly reduced (Fig. 8d). In addition, miR-310s and NOS deficiencies phenotypically copied, to a lesser extent, the cobblestone brain phenotype caused by Dg overexpression (Fig. 8e,f). Consistently, the milder brain phenotype in KT40 and ΔNOS mutants, relative to nervous system overexpression of Dg (insc > Dg), correlated with the measured Dg protein amounts (Supplementary Fig. 4b), again correlating that the severity of the brain dysplasia directly depends on the extent of Dg deregulation.

Similar to Dg mutant brains, cobblestone-like structures observed on miR-310s deficiency were also associated with aberrant cell adhesion protein expression (Supplementary Fig. 7). Importantly, the miR-310s mutant brain phenotype could be significantly rescued by reducing Dg levels (Fig. 8g). In addition, NO treatment had some positive effect on the brain outgrowth phenotype in Dg-overexpressing and NOS-deficient flies (Fig. 8g); however, it could not fully rescue it. This implies that some early NO-dependent developmental processes are irreversible and could not be repaired by transient NG administration. Taken together, these data show that the miR-310s promoter is responsive to the presence of higher amounts of Dg and NO signalling. This proposes that Dg is involved in transcriptional activation of the miR-310s via NO signalling, while NO signalling and the miR-310s in turn attenuate Dg abundance via a negative feedback loop.

Discussion

In summary, our data propose a novel perceptive-executive model for protein levels adjustment: it is perceptive, because it senses high levels of a critical protein, and it is executive, because it results in transcriptional activation of miRNAs that target the protein to restore its normal levels (Fig. 8h). As we showed, this regulation is potentially of great importance for stabilization of Dg expression levels, which modulates multiple cellular processes in the developing nervous system (Fig. 8h). As a consequence of miR-310s regulation, only a portion of Dg mRNAs with an extended 3′-UTR can be targeted, preventing Dg levels from being reduced below a certain threshold, which also is damaging for brain formation. Potentially, having a form of the target that is insensitive to miRNAs (alternatively processed 3′-UTR) allows adjustment of the target amount only to a critical level. Thus, the variability of 3′-UTR sequences has great significance in regulation of gene expression, where miRNAs act as managers of this extra layer of precision. Currently, the mechanisms coordinating alternative 3′-UTR processing for specific mRNA isoforms remain elusive; therefore, it would be important to understand what signalling controls the specifics of Dg 3′-UTR processing. Intriguingly, we found that the majority of the non-integrin ECM receptors have alternative 3′-UTRs that can be subjected to differential miRNA targeting (Table 1). This implies that the presented perceptive-executive model might be a more general buffering mechanism to readjust levels of essential molecules. Further, more detailed molecular evidence is required for the proposed here mechanism of protein expression regulation.

Alternative 3′-UTRs are common, sometimes tissue-specific, and often correlate with developmental stages, becoming shorter as the animal ages[30]. Recent bioinformatic work has shown that a high number of vertebrate mRNAs are alternatively polyadenylated and cleaved, leading to transcripts with different 3′-UTR lengths[39]. Interestingly, the longest 3′-UTRs among adult tissues are found in the brain[40–42] and 3′-UTR length also correlates with cell proliferation: tumour cells contain shorter 3′-UTRs[43]. Moreover, proliferating cells can have conserved mRNA transcripts with shorter 3′-UTRs in diverse cell types and tissues, and interestingly expression of the full-length 3′-UTRs results in reduced protein levels that can be reversed by mutating predicted miRNA target sites[44]. Therefore, the variability of 3′-UTR sequences offers an additional step, safeguarding the precision of gene expression where miRNAs play a key role. In this study, we report that Dg is subject to variable 3′-UTR processing and such processing determines its visibility to at least one family of miRNAs—the miR-310s. Interestingly, the 3′-UTR of the human Dg (DAG1) gene contains multiple miRNA binding sites and most of them are evolutionary conserved between vertebrates, suggesting that miRNA-based regulation of this important housekeeping gene might also take place in vertebrate organisms.

Prior studies in vertebrate muscle demonstrated that a signalling pathway involving DGC-regulated histone modification manages the proper transcription of miRNA genes[37]. In addition, regulation of mRNA levels is changed in human muscular dystrophies, correlating with mis-expressed miRNA–mRNA modules[45]. Interestingly, restoring of NO signalling or using histone deacetylase inhibitors return mis-expressed miRNAs to normal levels in mdx mice[46] and affectively ameliorate muscular dystrophy[47]. This proposes that the DGC via regulation of NO signalling maintains equilibrium between acetylation and deacetylation of histones and has an impact on muscle maintenance and/or the regenerative potential of muscle stem cells. In a miRNA microarray screen conducted on dystrophic flies, we found that on DGC deficit the expression profile of multiple miRNAs is altered[19]. Moreover, some of these miRNAs are predicted to be involved in multiple processes in the nervous system[19]. In addition, our study is the first report showing that Dg at least in Drosophila can be regulated posttranscriptionally via miRNAs in the nervous system. Here we propose that in the nervous system, Dg is able to regulate miRNA gene expression presumably via a NO-dependent mechanism. This implies that Dg and NO signalling can actively adjust epigenetic characteristics of neuronal cells. As Dg is also a signal-transducing module involved in crosstalk between the internal and external environments, this study suggests that Dg is involved in highly managed regulation of gene expression required to adapt cellular homeostasis that is compromised under dystrophic conditions. It would be important in the future to study in more detail how Dg via NO signalling manages gene expression in the nervous system.

We propose that Drosophila can be used as a model organism to study cobblestone lissencephaly, because Dg misregulation mutants present all typical syndromes associated with dystroglycanopathy: muscle degeneration[13,14], cobblestone brain and eye defects. Dystroglycanopathies are very pleiotropic, their associated pathologies range from very severe to few or no structural defects[48,49]. This wide symptomatic range can be explained by the nature of the mutations causing these neuromuscular disorders, which occur in multiple proteins that decorate the Dg glycoprotein with different sugars in a tissue-specific manner; other Dg modifications, such as phosphorylation and proteolysis, also have a profound effect on its physiological functions[6,23]. Thus, the common mechanism underlying the assortment of the defects observed in secondary dystroglycanopathies is abnormal cellular interaction with the ECM, composition of which is also altered due to abnormal α-Dg posttranslational modifications. Dg interacts with various laminins in a tissue- and cell type-specific manner, and

abnormal α-Dg posttranslational modifications generally alter the strength of neuron adhesion to the ECM. As our findings show that either decreased or increased Dg levels result in the cobblestone brain, we propose that proper brain architecture formation requires the intensity of Dg-coordinated cell–ECM interactions to be accurate. As cells produce their own ECM, there is bidirectional signalling between the extra- and intracellular machinery. For example, we showed that in *Drosophila*, Dg modulates the levels of the ECM protein laminin non-cell and cell autonomously, thus adjusting the ECM constitution to be in accordance with the amounts of Dg expressed by the cell[27].

The precision of cell adhesion protein expression is extremely important in the nervous system. Brain development, compart-mentalization and even synapse formation rely on the quantity and quality of cell adhesion molecules expressed by different types of neurons[50]. Based on expression patterns, we propose that there are different requirements for Dg as a cell adhesion receptor during different stages of neuron differentiation: first, to properly cluster, axons of fully differentiated neurons express certain levels of cell adhesion molecules; therefore, they have low, high or no Dg; second, to properly divide and differentiate, NBs, ganglion mother cells and not yet fully differentiated neurons readjust Dg levels according to their life cycle. In addition, we found that Dg is an important neuronal stem cell cycle regulator, as its misregulation leads to loss of cell cycle control in the brain. Together, our data show that the accuracy of neuronal proliferation, differentiation and axon pathfinding greatly depend on Dg levels and that miRNAs are candidates to buffer the levels of Dg expression against fluctuation in these processes. Overall, we believe that our *Drosophila* cobblestone lissencephaly model will allow for the better understanding of the molecular basis of dystroglycanopathies.

Methods

Fly strains and genetics. Fly stocks were maintained at 25 °C on a standard cornmeal-agar diet unless otherwise stated. The following *Drosophila* fly stocks were used: wild-type strain *Oregon-R-C* and *w1118* that were used as *Controls*; *GMR-Gal4, elav-Gal4, tub-Gal4, act-Gal4, D42-Gal4, 24B-Gal4, MHC-Gal4, wor-Gal4, insc-Gal4*, the deficiency spanning the *miR-310s* locus *DfExel6070* (Bloomington Drosophila Stock Center); and *UAS-Khc-73DP00530* (ref. 51). We used a *Gal4* insertion in the *miR-310s* locus, *P(GawB)NP4255* (referred to as *miR-310s-Gal4*), from Kyoto DGRC to analyse the *miR-310s* complex expression pattern[32]. We observed no phenotypes in homozygous flies with this insert and measured the levels of *miR-312* to be the same as in *Oregon R* flies. The *miR-310s* overexpression line (*UAS-miR-310s/TM6*) and deletion of *miR-310s* cluster line, *KT40* (ref. 32). For overexpression of Dg, we used transgenic lines containing the following constructs: *UASt-Dg*, which includes *Dg* full-length coding sequence, followed by truncated *Dg* 3′-UTR (670 bp, does not contain the *miR-310s* binding site); *UASt-DgΔExD*, which encodes truncated *Dg* that lacks the ECM binding domain[52]; and *UASt-Dg:GFP*, which contains GFP-tagged full-length *Dg* (used for immunoprecipitation analyses)[15]. For loss-of-function experiments, we used Dg mutants, *DgO86/CyO, DgO43/CyO, DgO38/CyO* and *DgO55/CyO*, and NOS mutant, *Nos415* (referred to as *ΔNOS*)[38]. The *UAS-mCD8-GFP, UAS-nLacZ* flies were kindly provided by Frank Hirth, and *hsFlp; Stau-GFP; act<FRT-CD2-FRT<Gal4, UAS-GFP* by Wu-Min Deng. To analyse the specificity of the phenotypes and to eliminate the possibility of a second site mutation, heteroallelic flies were analysed. All mutants and transgenes used in the experiments were compared with the control of the similar genetic background.

Lethality and development speed analyses. For embryonic lethality, flies were placed on agar plates with apple juice and allowed to lay eggs at 25 °C for 3–5 h and then the total number of eggs was counted. Embryos on plates were allowed to develop, and after 48 h the number of eggs that did not hatch was counted. The lethality was calculated by dividing the number of eggs that did not hatch by the total number of eggs. To analyse the viability and developmental delay caused by Dg loss-of-function *DgO86/CyO, DgO43/CyO* and *DgO38/CyO* lines were crossed to *DgO55/CyO* and the numbers of *Dg* homozygous versus *Dg* over *CyO* balancer heterozygous flies were counted during 5 days after flies started to eclose. *CyO/+* flies were intercrossed and their progeny were scored as *Controls*. As *Cy* is a lethal mutation, the expected ratio of *Cy* versus non-*Cy* flies should be 2:1. The per-centage of survival was calculated as ratio between the number of eclosed

homozygous flies divided by half of the number of eclosed flies with the *Cy* wing phenotype and multiplied by 100%.

Immunohistochemistry. Tissues were dissected and fixed in 4% formaldehyde. Antibody staining was performed as described before[14]. The following antibodies were used: rabbit anti-DgC-term[52] (1:2,000), rabbit anti-Dgex8 (ref. 53) (1:500), mouse anti-22C10, anti-β-Gal, anti-Elav, anti-βPS Integrin, anti-Pcan, anti-Arm, anti-Pros and rat anti-DE-Cad (1:50; Developmental Studies Hybridoma Bank), chicken anti-GFP (1:2,000; Abcam), rabbit anti-β-Gal (1:1,000; Invitrogen), rabbit anti-Phospho-Histone 3 (anti-PH3, 1:2,000; Upstate Biotechnologies), guinea pig anti-Miranda (gift from Andreas Wodarz, 1:1,000), rabbit anti-Caspase3 (1:200; Abcam), rabbit anti-LanB (1:1,000, Abcam ab47651), rabbit anti-Dys186 (gift from Lee Fradkin), Alexa 488/568 goat anti-mouse, Alexa 488/568/633 goat anti-rabbit, Alexa 488 goat anti-guinea pig, Alexa 568 goat anti-guinea pig, Alexa 488 goat anti-chicken (1:500; Invitrogen). Samples were mounted on slides in 70% glycerol, 2% n-propyl gallate, 1× PBS and analysed using a confocal microscope (Zeiss LSM 700). Quantification of staining intensities was done using the Zeiss software.

Histology. To prepare *Drosophila* tissue sections, flies were immobilized in collars in the required orientation and fixed in Carnoy fixative solution (6:3:1, ethanol: chloroform:acetic acid) at 4 °C overnight. Tissue dehydration and embedding in paraffin was performed as described previously[54]. Ten-micrometre histological sections were prepared using a Hyrax M25 (Zeiss) microtome and stained with haematoxylin and eosin. All chemicals for these procedures were obtained from Sigma Aldrich. Analysis was done using a light microscope (Zeiss).

Induction of loss- and gain-of-function clones. Females of genotype *hsFlp; act<FRT-CD2-FRT<Gal4, UAS-GFP* were crossed to males of genotype *UAS-miR-310s/TM6*. Two- to three-day-old females of the correct genotype were subjected to 1 h 37 °C heat-shock treatment for 2 consecutive days and put to fresh food with wet yeast for 3 days at which point ovaries were dissected and subjected to immunohistochemistry. To obtain Dg gain-of-function clones, *hsFlp; act<FRT-CD2-FRT<Gal4, UAS-GFP* were crossed either to *OregonR (Control)* or *UAS-Dg* flies and to obtain Dg loss-of-function clones; females of genotype *hsFlp; FRT42B Ubi-GFP/CyO* were crossed to males of genotype *w1118; FRT42B DgO86/CyO* or to parental *FRT 42B* as a control. F1 larvae from the cross were heat shocked for 2 h at 37 °C for 2 consecutive days and dissected as L3 to analyse the brains.

EdU labelling. To label cells that are in S phase, brains from L3 larvae where dissected in Schneider's *Drosophila* Medium (Life Technologies) and incubated in medium containing 0.01 μM EdU (5-ethyl-2′-deoxyuridine) for 1 h followed by fixation in 4% formaldehyde in 1× PBS for 20 min. Next, brain sections were washed two times with PBT (0.2% Triton X in 1× PBS) (20 min each) and blocked with PBTB (1× PBT, 0.2% bovine serum albumin, 5% normal goat serum, 0.05% sodium azide) for 30 min. Labelling of EdU-positive cells was performed using Click-iT EdU Alexa Fluor 555 Imaging Kit (Invitrogen/Molecular Probes) according to the manufacturer's protocol, followed by standard antibody staining protocol.

Nitroglycerin feeding. Thirsty 3- to 7-day-old adult flies were put overnight in vials containing filter paper soaked in 5% sucrose with 0.2 ng μl−1 NG (VWR EHERLA15586000AL) or just 5% sucrose (*Control*). 0.2 ng μl−1 was the con-centration of NG on which the lethality was <5%. Larvae were kept in vials with standard fly food supplemented with 500 μl of 5% sucrose with or without 0.2 ng μl−1 NG. L3 larvae were collected ~12 h after NG treatment.

Measurement of NO levels. To measure NO levels OxiSelect *in Vitro* Nitric Oxide Assay Kit was used (Cell Bioloabs STA-802). Measurements of total nitrite/nitrate amounts were done according to the manufacturer's protocol. Samples were prepared from three whole larvae in the standard western blotting lysis buffer.

In situ hybridization. Probes were designed to target the longer region of the 3′-UTR annotated in Flybase release FB2012_02 to belong to the *Dg-RD* transcript. Primers used to generate an ~350 bp sense fragment were: forward—5′-TAATA CGACTCACTATAGGGTCACGCAGTTAGTTATTCTC-3′ and reverse—5′-CAC ATAGACAAGAGTAAGTACAG-3′, where the underlined region corresponds with the T7 RNA polymerase promoter region. Primers used to generate an ~350 bp anti-sense fragment were: forward—5′-TCACGCAGTTAGTTATT CTC-3′ and reverse—5′-TAATACGACTCACTATAGGGCACATAGACAAGA GTAAGTACAG-3′.

Genomic DNA was PCR amplified using the above primers. One microgram of DNA in a 20-μl reaction was converted into RNA using a DIG RNA labelling kit (2 μl 10× transcription buffer, 2 μl 10× NTP labelling mixture (Roche), 1 μl RNase inhibitor (Applied Biosystems) and 2 μl of T7 RNA polymerase (New England Biolabs)). The reaction was carried out for 2 h at 37 °C. The solution was then treated with 2 μl of DNase1 (Invitrogen) for 15 min at 37 °C, and the reaction was stopped by the addition of 2 μl of 0.2 M EDTA. One microlitre of the solution

was run on an agarose gel to ensure that the RNA product was of the expected size. The probes were then stored at $-20\,°C$ in 10 µl of 1 M Tris pH 7.5 and 100 µl of hybridization buffer (50% formamide, 25% 20 × SSC, 5 mg ml^{-1} Torula yeast RNA (Sigma), 0.1% Tween 20) until their use.

Tissues were dissected, fixed for 30 min in 4% formaldehyde in PBS, dehydrated and stored at $-20\,°C$ overnight or longer. Tissues were then rehydrated, treated for 30 min to 1 h with Proteinase K solution (50 µg ml^{-1} Proteinase K in 50 mM Tris-HCl pH 7.5, 50 mM EDTA), and post-fixed in 4% formaldehyde in PBT for 30 min. Tissues were prehybridized for 1 h in hybridization buffer. Hybridization was carried out overnight at 60 °C with 2 µl per 100 µl of probe in hybridization buffer. Post hybridization washing was done at 62 °C with 3 subsequent 20-min washes with hybridization solution, 50/50 v/v hybridization solution/PBT, PBT. Tissues were then blocked for 1 h in Western Block (Sigma). Anti-DIG was diluted 1:2,000 in block and incubated with tissues overnight at 4 °C. Colorimetric detection was done with 10 µl ml^{-1} NBT (Roche) in staining buffer (0.05 M Tris pH 9.5, 0.05 M MgCl$_2$, 0.1 M NaCl, 0.1% Tween 20) for ~30–45 min. Analysis was done using Zeiss LSM 700 microscope.

PCR amplification of cDNAs. cDNA was generated as described above and subjected to standard PCR on a T100 Thermocycler (Bio-Rad) using the appropriate primers as described above to target the short and long *Dg* 3′-UTR, and to target the long *Dg* 3′-UTR. The PCR products were separated via electrophoresis on a 2% agarose gel. Densitometric analysis was used to determine the relative amounts of PCR products. Amplification efficiency was determined via densitometric analysis of the relative levels of unused primers for each reaction visualized at the bottom of the gel. PCR product levels were adjusted for the respective primer efficiencies and compared against one another to determine relative levels. The PCR product generated from primers that target both the short and long 3′-UTR were used as the normalizing quantity.

Reverse-transcription quantitative PCR. Total RNA was extracted using Trizol reagent (Invitrogen) following the manufacturer's protocol and treated with DNase1 (Invitrogen). To detect miRNA levels TaqMan microRNA assays (Applied Biosystems) were used to reverse transcribe from RNA and amplify cDNA specific to *miR-310, miR-311, miR-312, miR-313, miR-92a, miR-92b* and *2S rRNA* as an endogenous control on a StepOne Plus thermocycler (Applied Biosystems). Quantitative PCR (qPCR) was done using the Taqman qPCR master mix (Applied Biosystems). For the determination of transcript levels, mRNA was converted into cDNA using the High-Capacity reverse transcription kit (Applied Biosystems) following the manufacturer's directions. cDNA for *Dg* mRNA was amplified using the SYBR green master mix (Applied Biosystems). To detect *Dg* cDNA corresponding to the 3′-UTR long isoform, the forward and reverse primers were used respectively: 5′-TGGCTTCAATTGAGCGAGCT-3′ and 5′-TCACGCAGTTAGT TATTCTC-3′ (Fig. 3a). To detect *Dg* cDNA corresponding to the 3′-UTR long and short isoforms, following forward and reverse primers were used respectively: 5′-TTCACAAGCTCCCCTTTG GA-3′ and 5′-TCATTTCCCATCCTTCATGC AAC-3′ (Fig. 3a). As an endogenous control for all qPCR reactions, a product was also amplified corresponding to Ribosomal Protein L32 (RpL32) with the following forward and reverse primers respectively: 5′-AAGATGACCATCCGCCCAGC-3′ and 5′-GTCGATACCCTTGGGCTTGC-3′. All reactions were run at least in triplicate with appropriate blank controls. The threshold cycle (C_T) is defined as the fractional cycle number at which the fluorescence passes a fixed threshold. The ΔC_T value is determined by subtracting the average $RpL32$ or $2S$ $rRNA$ C_T value from the average tested C_T value. The $\Delta\Delta C_T$ value is calculated by subtracting the ΔC_T of the control sample from the ΔC_T of the suspect sample. The relative amount of mRNA or microRNA is then determined using the expression $2^{-\Delta\Delta CT}$.

Luciferase reporter assay. *Drosophila* S2R+ cells (DGRC Indiana) were seeded in a 96-well cell culture plate 1 day after splitting 1:5. Cells were transfected using the Effectene transfection reagent (Qiagen) with the following amounts: 50 ng of empty psiCHECK-2 (Promega) or 50 ng of psiCHECK-2 with the Dg-long-*3′-UTR* sensor cloned in, 25 ng of act-Gal4 and/or 50 ng of the pUAST-miR test plasmid. Approximately 72 h after transfection, the cells were subjected to the Dual-Glo luciferase assay (Promega). Both firefly (control reporter) and *Renilla* luciferase (altered 3′-UTR experimental reporter) levels were measured to achieve optimal and consistent results. Plates were analysed on a Wallac 1,420 luminometer. Non-transfected cells were used for blank subtraction from raw luminescence counts. The experimental reporter (*Renilla* luciferase) counts were divided by control reporter counts (*Firefly* luciferase) to determine the ratio of experimental/control reporter luminescence. The ratio of *Renilla* luciferase activity in the presence of the psiCHECK-2-Dg-3′-UTR plasmid with an appropriate *Dg* 3′-UTR fragment (P1–P4) was divided by the fold decrease in the presence of the empty psiCHECK-2 plasmid without the presence of transfected pUAST-miR plasmids to determine the downregulation ratio (control). Next, the *Renilla* luciferase activity was determined in the same way with the empty psiCHECK-2 and the psiCHECK-2-Dg-3′-UTR plasmid in the presence of the test pUAST-miR and the downregulation ratio between these values was calculated. The downregulation ratio of luminescence between the psiCHECK-2 plasmid and the psiCHECK-2-Dg-3′-UTR plasmid in the presence of the test pUAST-miR was then normalized to the downregulation ratio between the psiCHECK-2 plasmid and the psiCHECK-2-Dg-

3′-UTR plasmid without the test pUAST-miR to determine the relative reduction in *Renilla* luciferase expression caused by the presence of the test miRNA. The two-tailed Student's *t*-test was used to examine the significance of the effects statistically. All transfections were done three independent times to determine an average and s.e.m. The *DNA* plasmids *pUAST-miR-310s, pUAST-miR-312, pUAST-miR-313, pUAST-miR-92a* and *pUAST-miR-92b* were generated in the Lai lab[55] and obtained from the *Drosophila* Genomics Resource Center. To generate sensors for *Dg* 3′-UTR regions, fragments of interest were amplified from genomic *Drosophila melanogaster* DNA by PCR with primers that included enzymatic digestion sites for *NotI* and *XhoI* as follows: P1:*Dg*-3′-UTR: Fwd—5′-<u>TACGTGCGGCCGC</u>TTCGCAAATATTGGC-3′, Rev—5′-<u>CCACCATGGCTCGAGT</u>CCCTGAATCGAACT-3′; P2:*Dg*-3′-UTR: Fwd—5′-<u>TACGTGCGGCCGCG</u>TAGGTAGTAGTGTAGTAAG-3′, Rev—5′-<u>CCACCATGGCTCGAG</u>CATCAAAGGATCAGG-3′; P3:*Dg*-3′-UTR: Fwd—5′-<u>TACGTGCGGCCGC</u>TGGGACGATGGACATGTGTGC-3′, Rev—5′-<u>CCACCATGGCTCGAGG</u>CAGCAGGAAAGCAGCAAACC-3′; P4:*Dg-long*-3′-UTR: Fwd—5′-<u>TACGTGCGGCCGC</u>TCACGCAGTTAGTTATTCTC-3′, Rev—5′-<u>CCACCATGGCTCGAG</u>CCACATAGACAAGAGTAAGTACAG-3′, where the additional bases for enzyme cut sites are underlined. Fragments were subsequently cloned into *NotI* and *XhoI* restriction sites downstream of the *Renilla* luciferase gene in the psiCHECK-2 vector (Promega).

Western blotting. Sample preparation and SDS–PAGE have been described previously[56]. Bio-Rad ready-made 4–20% polyacrylamide gels were used for protein separation. Proteins were transferred to polyvinylidene difluoride membranes (BioRad) using a semi-dry transfer apparatus (Bio-Rad). Primary affinity-purified anti-Dg antibodies were used at 1:30,000. Goat anti-rabbit horseradish peroxidase-conjugated antibodies (Bio-Rad) were used as detection reagents at 1:10,000. Proteins were visualized via enhanced chemiluminescence (Millipore). Densitometry analysis was performed with the ImageJ programme. Uncropped scans of western blottings are provided in Supplementary Fig. 8.

Protein extraction and immunoprecipitation. Samples for immunoprecipitation were prepared from *Drosophila* larval brains that were homogenized and lysed in lysis buffer containing 50 mM Tris-HCl, 125 mM NaCl, 5% glycerol, 0.5% NP40, 0.25% Na-deoxycholate, 1.5 mM MgCl2, 1 mM dithiothreitol, 25 mM NaF, 1 mM Na₃VO₄, 1 mM EDTA, 2 mM EGTA and protease inhibitors. Samples where then centrifuged at 15,000*g* for 15 min at 4 °C. Protein extracts were pre-cleared with mouse IgG-agarose beads (Sigma) at 4 °C for 1 h. Supernatants were immuno-precipitated with GFP-Trap beads (ChromoTek) following the manufacturer's instructions. Ten per cent of total protein extracts used for immunoprecipitation was loaded as input. The presence of immunocomplexes was analysed via western blotting with LanB antibodies (1:10,000 Abcam).

References

1. Bryant, D. M. & Mostov, K. E. From cells to organs: building polarized tissue. *Nat. Rev. Mol. Cell. Biol.* **9,** 887–901 (2008).
2. Schwarz, U. S. & Gardel, M. L. United we stand - integrating the actin cytoskeleton and cell-matrix adhesions in cellular mechanotransduction. *J. Cell Sci.* **125,** 3051–3060 (2012).
3. Edeleva, E. & Shcherbata, H. R. Stress-induced ECM alteration modulates cellular microRNAs that feedback to readjust the extracellular environment and cell behaviour. *Front. Genet.* **4,** 305 (2013).
4. Ingber, D. E. Cellular mechanotransduction: putting all the pieces together again. *FASEB J.* **20,** 811–827 (2006).
5. Hoffman, E. P., Brown, Jr R. H. & Kunkel, L. M. Dystrophin: the protein product of the Duchenne muscular dystrophy locus. *Cell* **51,** 919–928 (1987).
6. Moore, C. J. & Winder, S. J. Dystroglycan versatility in cell adhesion: a tale of multiple motifs. *Cell Commun. Signal.* **8,** 3 (2010).
7. Koenig, M. *et al.* Complete cloning of the Duchenne muscular dystrophy (DMD) cDNA and preliminary genomic organization of the DMD gene in normal and affected individuals. *Cell* **50,** 509–517 (1987).
8. Marrone, A. K. & Shcherbata, H. R. Dystrophin orchestrates the epigenetic profile of muscle cells via miRNAs. *Front. Genet.* **2,** 64 (2011).
9. Bozzi, M., Morlacchi, S., Bigotti, M. G., Sciandra, F. & Brancaccio, A. Functional diversity of dystroglycan. *Matrix Biol.* **28,** 179–187 (2009).
10. Waite, A., Brown, S. C. & Blake, D. J. The dystrophin-glycoprotein complex in brain development and disease. *Trends Neurosci.* **35,** 487–496 (2012).
11. Devisme, L. *et al.* Cobblestone lissencephaly: neuropathological subtypes and correlations with genes of dystroglycanopathies. *Brain* **135,** 469–482 (2012).
12. Muntoni, F., Torelli, S., Wells, D. J. & Brown, S. C. Muscular dystrophies due to glycosylation defects: diagnosis and therapeutic strategies. *Curr. Opin. Neurol.* **24,** 437–442 (2011).
13. Shcherbata, H. R. *et al.* Dissecting muscle and neuronal disorders in a *Drosophila* model of muscular dystrophy. *EMBO J.* **26,** 481–493 (2007).
14. Kucherenko, M. M., Marrone, A. K., Rishko, V. M., Magliarelli Hde, F. & Shcherbata, H. R. Stress and muscular dystrophy: a genetic screen for dystroglycan and dystrophin interactors in *Drosophila* identifies cellular stress response components. *Dev. Biol.* **352,** 228–242 (2011).

15. Bogdanik, L. et al. Muscle dystroglycan organizes the postsynapse and regulates presynaptic neurotransmitter release at the Drosophila neuromuscular junction. PLoS ONE 3, e2084 (2008).

16. Marrone, A. K., Kucherenko, M. M., Rishko, V. M. & Shcherbata, H. R. New Dystrophin/Dystroglycan interactors control neuron behavior in Drosophila eye. BMC Neurosci. 12, 93 (2011).

17. Marrone, A. K., Kucherenko, M. M., Wiek, R., Gopfert, M. C. & Shcherbata, H. R. Hyperthermic seizures and aberrant cellular homeostasis in Drosophila dystrophic muscles. Sci. Rep. 1, 47 (2011).

18. Wairkar, Y. P., Fradkin, L. G., Noordermeer, J. N. & DiAntonio, A. Synaptic defects in a Drosophila model of congenital muscular dystrophy. J. Neurosci. 28, 3781–3789 (2008).

19. Marrone, A. K., Edeleva, E. V., Kucherenko, M. M. & Shcherbata, H. R. Dg-Dys-Syn1 signaling in Drosophila regulates the microRNA profile. BMC Cell. Biol. 13, 26 (2012).

20. Ibraghimov-Beskrovnaya, O. et al. Human dystroglycan: skeletal muscle cDNA, genomic structure, origin of tissue specific isoforms and chromosomal localization. Hum. Mol. Genet. 2, 1651–1657 (1993).

21. Dekkers, L. C. et al. Embryonic expression patterns of the Drosophila dystrophin-associated glycoprotein complex orthologs. Gene Expr. Patterns 4, 153–159 (2004).

22. Combs, A. C. & Ervasti, J. M. Enhanced laminin binding by alpha-dystroglycan after enzymatic deglycosylation. Biochem. J. 390, 303–309 (2005).

23. Inamori, K. et al. Dystroglycan function requires xylosyl- and glucuronyltransferase activities of LARGE. Science 335, 93–96 (2012).

24. Whitmore, C. et al. The transgenic expression of LARGE exacerbates the muscle phenotype of dystroglycanopathy mice. Hum. Mol. Genet. 23, 1842–1855 (2013).

25. Brancaccio, A. Alpha-dystroglycan, the usual suspect? Neuromuscul. Disord. 15, 825–828 (2005).

26. Schneider, M. et al. Perlecan and Dystroglycan act at the basal side of the Drosophila follicular epithelium to maintain epithelial organization. Development 133, 3805–3815 (2006).

27. Yatsenko, A. S. & Shcherbata, H. R. Drosophila miR-9a targets the ECM receptor Dystroglycan to canalize myotendinous junction formation. Dev. Cell 28, 335–348 (2014).

28. Michele, D. E. et al. Post-translational disruption of dystroglycan-ligand interactions in congenital muscular dystrophies. Nature 418, 417–422 (2002).

29. Acharyya, S. et al. Dystrophin glycoprotein complex dysfunction: a regulatory link between muscular dystrophy and cancer cachexia. Cancer Cell 8, 421–432 (2005).

30. Rice, K. M., Preston, D. L., Neff, D., Norton, M. & Blough, E. R. Age-related dystrophin-glycoprotein complex structure and function in the rat extensor digitorum longus and soleus muscle. J. Gerontol. Ser. A Biol. Sci. Med. Sci. 61, 1119–1129 (2006).

31. Lu, J. et al. Adaptive evolution of newly emerged micro-RNA genes in Drosophila. Mol. Biol. Evol. 25, 929–938 (2008).

32. Tsurudome, K. et al. The Drosophila miR-310 cluster negatively regulates synaptic strength at the neuromuscular junction. Neuron 68, 879–893 (2010).

33. Wu, C. I., Shen, Y. & Tang, T. Evolution under canalization and the dual roles of microRNAs: a hypothesis. Genome Res. 19, 734–743 (2009).

34. Petrof, B. J., Shrager, J. B., Stedman, H. H., Kelly, A. M. & Sweeney, H. L. Dystrophin protects the sarcolemma from stresses developed during muscle contraction. Proc. Natl Acad. Sci. USA 90, 3710–3714 (1993).

35. Wehling, M., Spencer, M. J. & Tidball, J. G. A nitric oxide synthase transgene ameliorates muscular dystrophy in mdx mice. J. Cell Biol. 155, 123–131 (2001).

36. Ervasti, J. M. & Sonnemann, K. J. Biology of the striated muscle dystrophin-glycoprotein complex. Int. Rev. Cytol. 265, 191–225 (2008).

37. Cacchiarelli, D. et al. MicroRNAs involved in molecular circuitries relevant for the Duchenne muscular dystrophy pathogenesis are controlled by the dystrophin/nNOS pathway. Cell Metab. 12, 341–351 (2010).

38. Yakubovich, N., Silva, E. A. & O'Farrell, P. H. Nitric oxide synthase is not essential for Drosophila development. Curr. Biol. 20, R141–R142 (2010).

39. Tian, B., Hu, J., Zhang, H. & Lutz, C. S. A large-scale analysis of mRNA polyadenylation of human and mouse genes. Nucleic Acids Res. 33, 201–212 (2005).

40. Beaudoing, E. & Gautheret, D. Identification of alternate polyadenylation sites and analysis of their tissue distribution using EST data. Genome Res. 11, 1520–1526 (2001).

41. Smibert, P. et al. Global patterns of tissue-specific alternative polyadenylation in Drosophila. Cell Rep. 1, 277–289 (2012).

42. Hilgers, V. et al. Neural-specific elongation of 3' UTRs during Drosophila development. Proc. Natl Acad. Sci. USA 108, 15864–15869 (2011).

43. Clancy, J. L. et al. mRNA isoform diversity can obscure detection of miRNA-mediated control of translation. RNA 17, 1025–1031 (2011).

44. Sandberg, R., Neilson, J. R., Sarma, A., Sharp, P. A. & Burge, C. B. Proliferating cells express mRNAs with shortened 3' untranslated regions and fewer microRNA target sites. Science 320, 1643–1647 (2008).

45. Eisenberg, I. et al. Distinctive patterns of microRNA expression in primary muscular disorders. Proc. Natl Acad. Sci. USA 104, 17016–17021 (2007).

46. Greco, S. et al. Common micro-RNA signature in skeletal muscle damage and regeneration induced by Duchenne muscular dystrophy and acute ischemia. FASEB J. 23, 3335–3346 (2009).

47. Pescatori, M. et al. Gene expression profiling in the early phases of DMD: a constant molecular signature characterizes DMD muscle from early postnatal life throughout disease progression. FASEB J. 21, 1210–1226 (2007).

48. Moore, S. A. et al. Deletion of brain dystroglycan recapitulates aspects of congenital muscular dystrophy. Nature 418, 422–425 (2002).

49. Satz, J. S. et al. Distinct functions of glial and neuronal dystroglycan in the developing and adult mouse brain. J. Neurosci. 30, 14560–14572 (2010).

50. Kucherenko, M. M. & Shcherbata, H. R. Steroids as external temporal codes act via miRNAs and cooperate with cytokines in differential neurogenesis. Fly (Austin) 7, 173–183 (2013).

51. Staudt, N. et al. Gain-of-function screen for genes that affect Drosophila muscle pattern formation. PLoS Genet. 1, e55 (2005).

52. Deng, W. M. et al. Dystroglycan is required for polarizing the epithelial cells and the oocyte in Drosophila. Development 130, 173–184 (2003).

53. Schneider, M. & Baumgartner, S. Differential expression of Dystroglycan-spliceforms with and without the mucin-like domain during Drosophila embryogenesis. Fly. (Austin, Tex) 2, 29–35 (2008).

54. Kucherenko, M. et al. Paraffin-embedded and frozen sections of Drosophila adult muscles. JoVE 46 (2010).

55. Silver, S. J., Hagen, J. W., Okamura, K., Perrimon, N. & Lai, E. C. Functional screening identifies miR-315 as a potent activator of Wingless signaling. Proc. Natl Acad. Sci. USA 104, 18151–18156 (2007).

56. Yatsenko, A. S. et al. A putative Src homology 3 domain binding motif but not the C-terminal dystrophin WW domain binding motif is required for dystroglycan function in cellular polarity in Drosophila. J. Biol. Chem. 282, 15159–15169 (2007).

57. Kauffmann, R. C., Li, S., Gallagher, P. A., Zhang, J. & Carthew, R. W. Ras1 signaling and transcriptional competence in the R7 cell of Drosophila. Genes Dev. 10, 2167–2178 (1996).

58. Kheradpour, P., Stark, A., Roy, S. & Kellis, M. Reliable prediction of regulator targets using 12 Drosophila genomes. Genome Res. 17, 1919–1931 (2007).

Acknowledgements

Author contributions

A.S.Y., A.K.M. and H.R.S.: conception and plan of the work, data acquisition, analysis and interpretation, figure design and manuscript draft.

Additional information